© 2020. Published by The Company of Biologists Ltd | Development (2020) 147, dev181305. doi:10.1242/dev.181305

RESEARCH ARTICLE

WNT regulates programmed muscle remodeling through PLC-β and calcineurin in *Caenorhabditis elegans* males

Brigitte LeBoeuf*, Xin Chen* and Luis Rene Garcia‡

ABSTRACT

The ability of a muscle to break down and reform fibers is vital for development; however, if unregulated, abnormal muscle remodeling can occur, such as in the heart following cardiac infarction. To study how normal developmental remodeling is mediated, we used fluorescently tagged actin, mutant analyses, Ca^{2+} imaging and controlled Ca^{2+} release to determine the mechanisms regulating a conspicuous muscle change that occurs in *Caenorhabditis elegans* males. In hermaphrodites and larval males, the single cell anal depressor muscle, used for waste expulsion, contains bilateral dorsal-ventral sarcomeres. However, prior to male adulthood, the muscle sex-specifically remodels its sarcomeres anteriorly-posteriorly to promote copulation behavior. Although WNT signaling and calcineurin have been implicated separately in muscle remodeling, we unexpectedly found that they participate in the same pathway. We show that WNT signaling through Gαo and PLC-β results in sustained Ca^{2+} release via IP_3 and ryanodine receptors to activate calcineurin. These results highlight the utility of this new model in identifying additional molecules involved in muscle remodeling.

KEY WORDS: G-protein-coupled signaling, Muscle remodeling, WNT/Calcium signaling, WNT/PCP signaling

INTRODUCTION

Muscle remodeling is an important part of development and disease progression (Freire et al., 2014). In development, muscles must reshape as the organism's needs change. In adults, detrimental events, such as cardiac infarction, can lead to dormant developmental pathways re-activating, which reshapes heart muscle to a pathological degree. To prevent and treat abnormal remodeling, normal well-regulated developmental remodeling must be studied to determine how molecular pathways control this process.

The *Caenorhabditis elegans* male provides one such opportunity for study as one of its tail muscles undergoes a drastic sex-specific remodeling event during larval to adult development (Jarrell et al., 2012; Sulston et al., 1980; Sulston and Horvitz, 1977). The single cell anal depressor muscle, located in the male tail, goes through a complete remodeling in both structure and function during larval development. In the early larval (L1-L3) male, this muscle contains a dorsal-ventral sarcomere that participates in defecation. During the last larval stage (L4), the muscle remodels. In the adult male, it contains an anterior-posterior sarcomere that positions the copulatory spicule during male mating behavior, facilitating sperm transfer into the hermaphrodite uterus (LeBoeuf and Garcia, 2017). This muscle remodeling takes place concurrently with the morphogenesis of male copulatory structures (Sulston et al., 1980). In contrast, the hermaphrodite anal depressor does not remodel and remains a defecation muscle. We previously reported that the sexual identity of the anal depressor is necessary for developmental remodeling (Chen and García, 2015). However, the pathways regulating this process are unidentified.

Here, we report that multiple WNT pathways are necessary for sarcomere remodeling. During early development, the WNT planar cell polarity (PCP) pathway is required in epithelial cells that neighbor the anal depressor. Later in development, the WNT/calcium pathway has WNT ligands acting directly on the anal depressor, promoting G-protein-coupled signaling that is dependent on Gαo and Gα/GPA-7. This leads to PLC-β activation, which triggers calcium release from internal stores through IP_3 and ryanodine receptors. Calcium signaling then promotes the calcium/calmodulin-dependent phosphatase calcineurin to further facilitate the morphogenesis of the anal depressor.

RESULTS

Sarcomere remodeling during male L4 to adult development

Our previous study established that the extensive remodeling of the male anal depressor, which occurs during L4 development, is dependent upon the sexual identity of the muscle (Chen and García, 2015; Jarrell et al., 2012; Garcia et al., 2001; Reiner and Thomas, 1995; Sulston et al., 1980). Problematically, the work used a YFP:actin construct (driven by the *unc-103E* promoter) that is also expressed in the sex muscles, which partially obscure the adult anal depressor (Chen and García, 2015; Reiner et al., 2006). To visualize the anal depressor more clearly in adults, we generated an integrated YFP:actin construct that uses the *aex-2* promoter, which is expressed in the anal depressor, sphincter, intestinal muscles and the motor neuron DVB, but not in the male sex muscles (Fig. 1) (Mahoney et al., 2008). The P*aex-2*:YFP:actin construct allowed clearer dissection of anal depressor remodeling.

In both hermaphrodites and larval males, the single cell anal depressor had left and right sarcomeres that spanned from the dorsal cuticle to the ventral anus (Fig. 1A,B). The sarcomeres contract during the last step of defecation, allowing expulsion of the gut contents (Thomas, 1990). Although similar in form and function, the larval male anal depressor did not expand like the hermaphrodite muscle (Fig. 1C-D′) (Chen and García, 2015). During the last larval stage (L4), the sarcomeres in the male anal depressor underwent a dramatic reorganization, so that the cell transformed from a dorsal-ventral defecation muscle to an anterior-posterior auxiliary mating muscle. First, during late L3 to early L4 larval stage, a ventral slit formed along the rectal attachment, demarking the anterior and posterior domains (Fig. 1E,E′). The domain anterior to the slit elongated along the neighboring epithelia to attach to the

Department of Biology, Texas A&M University, College Station, TX 77843, USA.
*These authors contributed equally to this work

‡Author for correspondence (rgarcia@bio.tamu.edu)

B.L., 0000-0003-4155-2533; L.R.G., 0000-0003-3087-6989

Handling Editor: Susan Strome
Received 7 June 2019; Accepted 31 March 2020

Development (2020) 147, dev181305. doi:10.1242/dev.181305

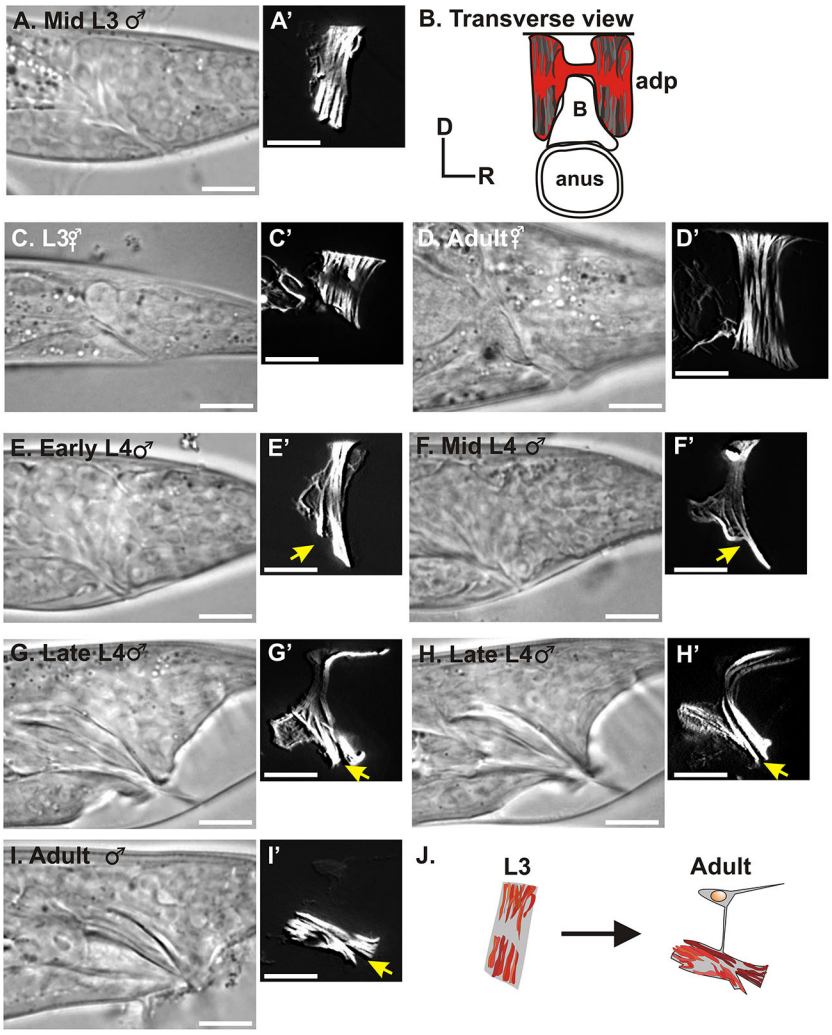

Fig. 1. Visualization of male anal depressor rearrangement using YFP:actin. (A,A′,E-I′) DIC (A,E,F,G,H,I) and fluorescent (A′,E′,F′,G′,H′,I′) images of the male tail. The arrows in the fluorescent images point to the ventral slit that denotes the anterior and posterior domains. (B) Diagram representing the transverse view of the hermaphrodite and larval male anal depressor (adp). The sarcomere orientation is indicated by the gray shading. There are two dorsal attachments, left and right. D, dorsal; R, right. (C-D′) DIC (C,D) and fluorescent (C′,D′) images of the hermaphrodite tail. (J) Diagram of the male anal depressor representing both the actin (red lines) and cell shape (in gray). The location of the nucleus is in yellow. For all images except B, dorsal is up and anterior is to the left. Scale bars: 10 µm.

developing spicule protractor muscles (Fig. 1F; Fig. S1). While this occurs, the dorsal-ventral sarcomere in the posterior domain was present and was not fully disassembled until the end of L4 (Fig. 1G-I′). The fluorescently tagged actin from the P*aex-2*:YFP:actin integration showed a similar disassembly process to the P*unc-103*E:YFP:actin transgene (Fig. 1) (Chen and García, 2015). Interestingly, we noted that each left and right dorsal-ventral sarcomere was reorganized into two partially overlapping anterior-posterior sarcomeres, a feature that was not seen with the P*unc-103E*:YFP:actin construct (Fig. 1J; Fig. S2).

WNT ligands and receptor regulate anal depressor rearrangement

To determine which developmental pathways are used for *C. elegans* male anal depressor rearrangement, we generated an integrated transgenic line expressing cytoplasmic YFP from the *aex-2* promoter. YFP expression was diffuse throughout the cell, showing both the ventrally located muscle attachments and the dorsally located nucleus (Fig. 2A). We crossed this marker to strains defective in different developmental pathways, including EGF/LIN-3 (Fig. 2B), notch/LIN-12 (Fig. 2C), TGFβ/SMA-6 (Fig. 2D) and

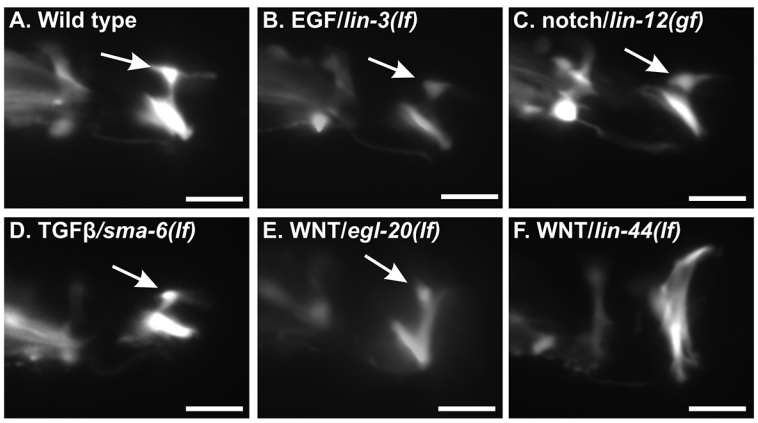

Fig. 2. Anal depressor rearrangement defects in developmental mutants. (A-F) YFP fluorescent images of the anal depressor muscle in wild-type (A) and mutant (B-F) adult male tails. Dorsal is up and posterior is to the right. Arrows point to the location of the cell body. In F, the cell body is hidden in the abnormal anal depressor. Scale bars: 10 µm.

Development (2020) 147, dev181305. doi:10.1242/dev.181305

WNT ligands (EGL-20, LIN-44). Only mutations in the WNT pathway ligands showed anal depressor rearrangement defects (Fig. 2E,F), suggesting that WNT signaling is involved in anal depressor remodeling.

The cytoplasmic YFP only shows the overall morphology of the anal depressor, not sarcomere-specific defects. As depicted in Fig. 1, the entire dorsal-ventral sarcomere of the developing male tail is remodeled into anterior-posterior sarcomeres, necessitating sarcomere disassembly. To determine the state of the anal depressor sarcomere in WNT mutants, we crossed the P*aex-2*:YFP:actin integration into WNT mutant backgrounds. The dorsal-ventral sarcomere in early wild-type L4 males, immediately before disassembly begins, is ∼9 µm, whereas the hermaphrodite anal depressor around the same developmental stage is ∼14 µm (Chen and García, 2015). However, by the time the males are adults, no dorsal-ventral sarcomere should be present (Fig. 3A), meaning that any remaining dorsal-ventral sarcomere indicates incomplete disassembly. Mutant males could have minor defects, where most of the dorsal-ventral sarcomere disassembles but some remained (Fig. 3B), to more severe defects, where a significant portion of the dorsal-ventral sarcomere did not disassemble (Fig. 3C), and finally to a complete lack of disassembly (Fig. 3D). We counted the number of males with normal and defective sarcomeres (Fig. 3E). Any male that had even minor defects was considered mutant. In addition, we also measured the dorsal-ventral sarcomere width (Fig. 3F), and reported that measurement, where necessary, to highlight differences in severity between mutants.

Three WNT ligands are expressed in the tail: LIN-44, EGL-20, and CWN-1 (Pan et al., 2006; Whangbo and Kenyon, 1999; Herman et al., 1995). Whereas *cwn-1* loss-of-function (lf) mutant males showed occasional minor defects, defects in *lin-44(lf)* and *egl-20(lf)* mutant males were more severe (Fig. 3E). Some sarcomere disassembly occured but was not always completed, and the anterior-posterior sarcomere was formed but was not always wild type (Fig. 3B,C). Thus, *lin-44* and *egl-20*-encoded ligands are probably the primary drivers of WNT-regulated anal depressor rearrangement in the developing male tail.

WNT ligands EGL-20 and LIN-44 both activate the frizzled receptor, which is encoded by *lin-17* (Sawa et al., 1996). LIN-17 functions in early male tail development (Wu and Herman, 2007, 2006), therefore it might be involved in anal depressor rearrangement. When we expressed YFP:actin in *lin-17(lf)* mutants, we found that they displayed more severe defects than any of the WNT ligands alone (Fig. 3D,F). In many males, no disassembly occurred, and the anterior-posterior sarcomere was never formed (Fig. 3D,F). Thus, *lin-17* is a WNT receptor involved in anal depressor rearrangement. As the mutant frizzled receptor phenotype is more severe than *lin-44(lf)* or *egl-20(lf)*, we created a double WNT ligand mutant and observed that *lin-44(lf); egl-20(lf)* males displayed similar defects to *lin-17(lf)* males (Fig. 3F). Any differences in disassembly defects between the *lin-44(lf); egl-20(lf)* double mutant and *lin-17(lf)* single mutant might be accounted for by minor compensation from *cwn-1*. Thus, LIN-44 and EGL-20 promote sarcomere disassembly through LIN-17.

We examined the location of *lin-17* expression using the *lin-17* promoter to drive YFP. We determined that *lin-17* was expressed in both hermaphrodite and male anal depressors from an early stage (Fig. 3G,H, Fig. S3A). Because of its expression pattern, we investigated whether *lin-17* also plays a role in the hermaphrodite anal depressor. We measured the dorsal-ventral sarcomere width of wild-type and mutant hermaphrodites, and determined that *lin-17(lf)* mutant hermaphrodites lacked anal depressor symmetry (Fig. 3I); this asymmetry was also seen in males (Fig. 3J). Thus, *lin-17* is also required in both sexes for maintaining anal depressor symmetry during development.

To confirm that a reduction in the number of of frizzled/LIN-17 receptors leads to the defective anal depressor, we generated a *lin-17* cDNA rescuing construct. We used the endogenous *lin-17* promoter to drive expression in male tail cells, including the anal depressor and the epithelial cells (the B cell and its descendants) that the muscle attaches to as it remodels (Sawa et al., 1996). These B-derived cells produce the male copulatory spicules, associated neurons and the proctodeum. Some of these cells also provide the substrate to which the copulatory muscles, including the anal depressor, attach (Sulston et al., 1980). We injected the P*lin-17*:*lin-17* construct into *lin-17(lf)* mutant worms and rescued the anal depressor defects (Fig. 3K, Fig. S3B), confirming that LIN-17 is involved in male anal depressor rearrangement.

We next investigated where in the male tail *lin-17* expression was important for sarcomere disassembly. To address this question, we expressed *lin-17* in a variety of tissues in the *lin-17(lf)* mutant male tail, including the sex muscles (using the P*unc-103*E promoter), the anal depressor (using the P*aex-2* promoter) and the rectal epithelial cells that neighbor the anal depressor (using the P*pop-1* promoter). At the L1 stage, the *pop-1* promoter expresses in the B cell, its descendants B.a and, to a lesser extent, B.p (Fig. S3C-G) (Wu and Herman, 2006); the *pop-1* promoter does not drive expression in the anal depressor. Expressing *lin-17* in the sex muscles or anal depressor had no impact on the *lin-17(lf)* phenotype (Fig. 3K, Fig. S3B). However, expressing *lin-17* in the rectal epithelial B-cell descendants did reduce the severity of the defect severity but not the penetrance (Fig. 3K, Fig. S3B). As restoring *lin-17* in the rectal epithelial cells partially rescued the anal depressor defect, we checked whether co-expressing *lin-17* in multiple locations could improve rescue. Indeed, we found that expressing *lin-17* in both the rectal epithelial cells and the anal depressor of *lin-17* mutants produced a better rescue than either one alone (Fig. 3K). This result indicates that *lin-17* functions both in the anal depressor and the neighboring rectal epithelial cells to promote sarcomere disassembly.

We suggest that the reason the P*pop-1*:*lin-17* transgene can rescue the *lin-17(lf)* disassembly defects is due to it restoring the patterning of the B cell descendants. When these epithelial cells are patterned correctly, they can provide the proper structural substrate necessary for the anal depressor to rearrange. The B cell does not divide in hermaphrodites and this is the reason that their anal depressor does not remodel. In males, LIN-17 is required for early asymmetrical cell divisions that establish the fates of these epithelial cells (Wu and Herman, 2007, 2006). The epithelial cells are all descendants of the B cell, a large cell in the male tail during the L1 developmental stage (Fig. S3C-E). This cell divides into anterior and posterior cells (B.a and B.p), with B.a being larger than B.p. This asymmetry is dependent on *lin-17* (Wu and Herman, 2006). Following this cell division, the anal depressor is located over B.p (Fig. S3E,H) (Barr et al., 2018). During the L2 and L3 stages, the B.p cell divides further, with the anal depressor eventually maintaining contact with the B.paa and B.pap descendants (Barr et al., 2018) (Fig. S3I).

To further support a role for the B cell descendants in anal depressor rearrangement, we laser-ablated the B cell descendants that directly contact the anal depressor (B.pa or B.paa and B.pap) in wild-type larval males. Although these B cell descendants should be patterned by the time of ablation, the anal depressor in a significant number of operated males failed to disassemble (Fig. S3J). We could not analyze the results of operations conducted at an earlier developmental time,

Development (2020) 147, dev181305. doi:10.1242/dev.181305

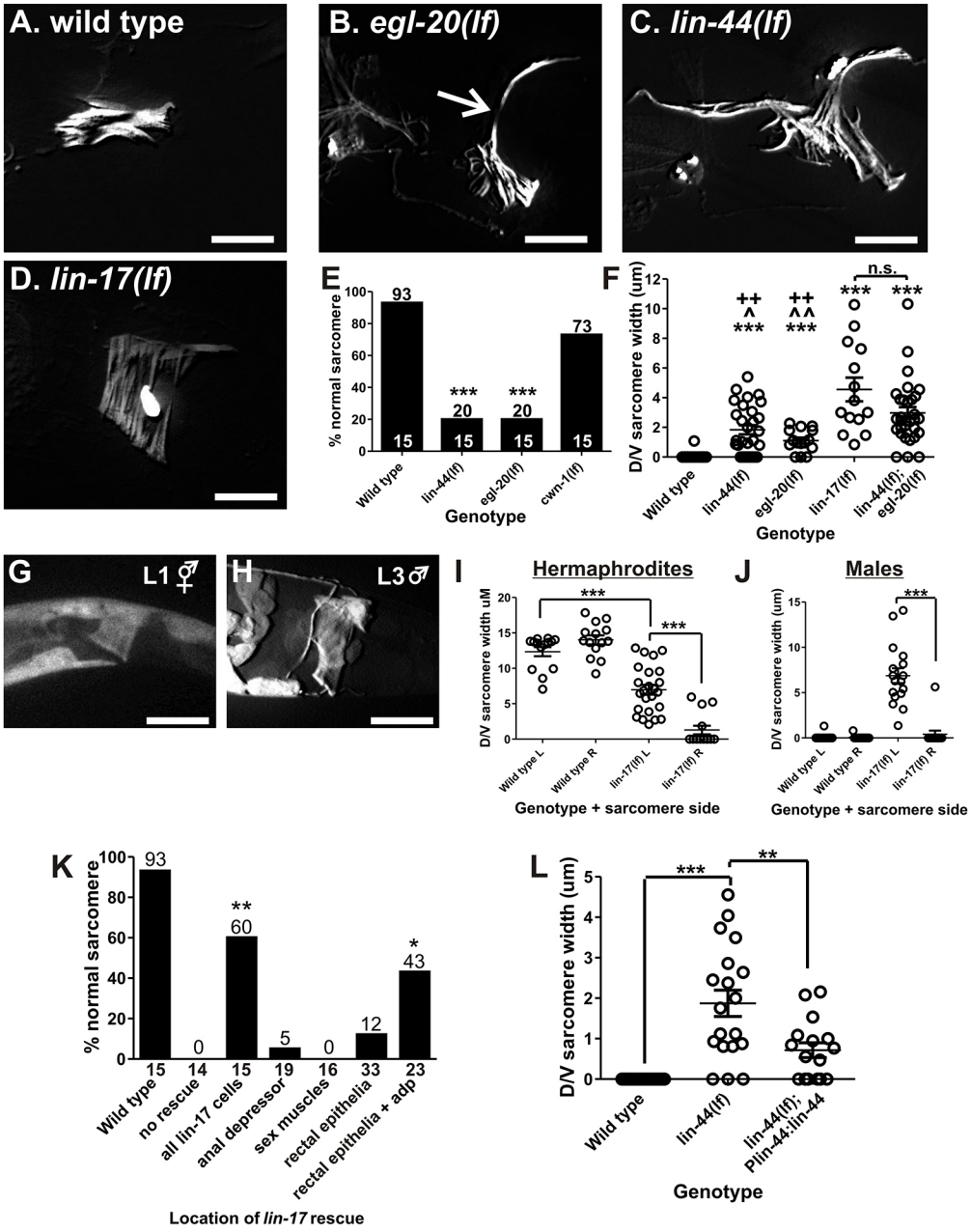

Fig. 3. WNT mutant anal depressor defects. (A-D) Fluorescent image of YFP:actin in the wild-type (A), *egl-20(lf)* (B), *lin-44(lf)* (C) and *lin-17* (D) anal depressors. The arrow in B indicates dorsal-ventral sarcomere width measured in F,I,J and L. (E) Graph depicting the percentage of males with normal sarcomeres in the indicated mutants. Numbers above the bars give the percentage and numbers above the *x*-axis represent the total sample number for each line. ****P*<0.0001, Fisher's exact test, compared with wild type. (F) Graph depicting the severity of the remodeling defects. Each circle represents the dorsal/ventral sarcomere width of either the left or right dorsal attachment in one male (see arrow in B). Data are mean±s.e.m. ****P*<0.0001, Mann–Whitney *t*-test compared with wild type. ^*P*<0.05, ^^*P*<0.005, Mann–Whitney *t*-test compared with *lin-44(lf);egl-20(lf)*. ++*P*<0.005, Mann–Whitney *t*-test compared with *lin-17(lf)*. n.s., not significant. (G,H) Fluorescent images of YFP expressed from the *lin-17* promoter. The anal depressor is at the center of the image. (I,J) Left (L) and right (R) dorsal-ventral sarcomere width in adult anal depressors. Each circle represents the width of the sarcomere on the indicated side of an individual animal. ****P*<0.0001, Mann–Whitney *t*-test. (K) Graph depicting the percentage of males with normal sarcomeres. The *x*-axis indicates where wild-type *lin-17* cDNA is expressed. The numbers on top of the bars represent the percentages. The number below the *x*-axis represents the total sample number for each location. **P*<0.05, ***P*<0.005, Fisher's exact test, compared with no rescue. (L) *lin-44(lf)* anal depressor defects are rescued with a transgene. Each circle represents the dorsal/ventral sarcomere width of either the left or right dorsal attachment in one male (see arrow in C). Data are mean±s.e.m. ***P*<0.005, ****P*<0.0001, Mann–Whitney *t*-test. For all images, dorsal is up and anterior is to the left. Scale bars: 10 µm.

as ablating the B or B.p cells results in the intestine herniating through the rectum. Nonetheless, our results indicate a role for the B cell descendants in anal depressor remodeling.

Previous work established that LIN-17 on the B cell descendant membranes was stimulated by the WNT ligand LIN-44 (Wu and Herman, 2006). Our analysis of *lin-44(lf)* mutants indicated that the ligand promotes proper anal depressor rearrangement (Fig. 3E,F). To confirm this result, in *lin-44(lf)* mutants we rescued *lin-44* expression using the genomic sequence and its own promoter. This construct was able to significantly reduce the sarcomere

Development (2020) 147, dev181305. doi:10.1242/dev.181305

rearrangement defect (Fig. 3L). However, although the defects were not as severe, they were still present. This was probably a result of either mosaicism of the transgene or over-expression of WNT. Both over-expression and reduction of WNT signaling are capable of causing mutant phenotypes (Kirszenblat et al., 2011; Pénigault and Félix, 2011; Pan et al., 2006).

Cell-autonomous membrane-tethered *egl-20*/WNT can promote sarcomere disassembly

Previous work established that WNT/LIN-44 activates frizzled/LIN-17 on the developing posterior rectal epithelial cells to establish male-specific structures (Wu and Herman, 2006). However, as *lin-44(lf)* mutant defects are not as severe as *lin-17(lf)* mutant defects, an additional WNT ligand must also function in the male tail. The other WNT ligand is EGL-20, as the severity of the *lin-44(lf); egl-20(lf)* double mutant is similar to that of the *lin-17(lf)* mutant. Additionally, we showed that the *lin-17(lf)* muscle remodeling defect is best rescued through expression of wild-type *lin-17* in the epithelial cells and the anal depressor. As LIN-44 is the WNT ligand that specifies B-cell descendant asymmetry, EGL-20 might be the WNT ligand acting on the anal depressor.

To determine where *egl-20* is functionally expressed, we made a reporter construct containing the genomic *egl-20* locus that starts at the ATG, ends after the 3′ UTR, and contains an SL2 trans-spliced red fluorescent protein (RFP). Expression of *egl-20* occurs in the anal depressor, the rectal epithelial cells neighboring the anal depressor and the sex muscles in the male tail (Harterink et al., 2011; Whangbo and Kenyon, 1999) (Fig. 4A-B″). We placed the *egl-20* promoter in front of our *egl-20* genomic construct and injected this DNA into *egl-20(lf)* mutants; this DNA successfully rescued the disassembly defects (Fig. 4C). Expressing *egl-20* in either the anal depressor (via the *aex-2* promoter) or the rectal epithelial cells (via the *pop-1* promoter) also rescued the *egl-20(lf)* phenotype (Fig. 4C). Thus, *egl-20* can be provided by multiple male tail cells to regulate anal depressor remodeling.

WNT is primarily known to function as a secreted ligand (Pani and Goldstein, 2018); however, WNT can rescue many WNT-deficient defects as a membrane-tethered ligand (Alexandre et al., 2014). To determine whether WNT has to be secreted or can act as a membrane-tethered ligand in anal depressor remodeling, we fused a membrane-spanning domain of PAT-3 integrin to the C-terminus of EGL-20 (Gettner et al., 1995). We then expressed this construct in the anal depressor (via the *aex-2* promoter) of the *egl-20(lf)* mutants and determined that it is capable of rescuing disassembly defects (Fig. 4C). Expressing membrane-tethered WNT in the adjacent epithelial cells (via the *pop-1* promoter) failed to rescue these defects (Fig. 4C). Therefore, although secreted WNT from multiple sources can promote sarcomere remodeling, rescue of the *egl-20(lf)* phenotype by membrane-tethered WNT can only be accomplished if it is expressed in the anal depressor itself. Although this experiment cannot address how WNT functions normally (as a secreted ligand, membrane-tethered ligand or both), the failure of epithelial-expressed membrane-tethered WNT to rescue *egl-20(lf)* defects suggests that WNT must be in a form that can be internalized in the anal depressor. Unlike the membrane-tethered anal depressor WNT, which can bind to its cell-autonomous receptor and be internalized, anchoring WNT to the surrounding cells probably obstructs its proper interaction with the muscle-expressed LIN-17 and subsequent internalization.

WNT/β-catenin pathways are involved in anal depressor rearrangement

Canonical WNT signaling through β-catenin is involved in many *C. elegans* developmental processes (Sawa and Korswagen, 2013). Thus, we investigated whether β-catenin participates in anal

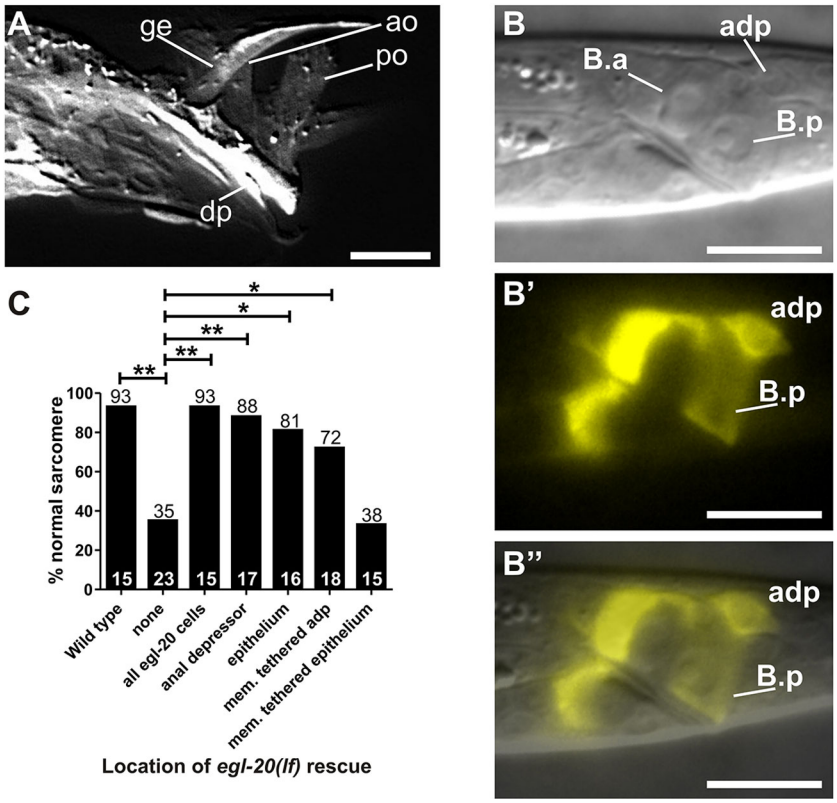

Fig. 4. WNT/EGL-20 ligand functions in the tail to regulate anal depressor rearrangement. (A-B″) *egl-20* expression pattern in males. (A) Confocal DsRed1-E5 fluorescent image of an adult male. DIC L2 male (B) and *egl-20*-expressed RFP fluorescent images (B′) are shown separately. B″ shows these images stacked on top of one another, to highlight where *egl-20* is expressed. (C) Graph depicting the percentage (numbers on top of the basr) of males with normal sarcomeres. The *x*-axis indicates where wild-type *egl-20* genomic DNA is expressed. The numbers above the *x*-axis represent the total sample number for each location. **P*<0.05, ***P*<0.005, Fisher's exact test. For all images, dorsal is up and anterior is to the left. adp, anal depressor; ge, gubernaculum erector; ao, anterior oblique; po, posterior oblique; dp, dorsal protractor. Scale bars: 10 µm.

Development (2020) 147, dev181305. doi:10.1242/dev.181305

depressor remodeling. *C. elegans* has four β-catenin genes: *bar-1*, *hmp-2*, *sys-1* and *wrm-1*. Owing to the *bar-1* locus being on the same chromosome (X) as our integrated P*aex-2*:YFP:actin reporter construct, we could not easily use canonical *bar-1* mutations. Instead, we used CRISPR/Cas9 to generate a new *bar-1* allele, *rg804*, in our integrated P*aex-2*:YFP:actin background. This allele has a 4 bp deletion that results in the loss of a lysine at amino acid 45, creating a frame shift that leads to a stop codon 15 amino acids downstream of the mutation. This allele produces defects associated with *bar-1* loss-of-function mutants in hermaphrodites, such as uncoordinated movement and reduced egg-laying behavior. Despite this, *bar-1(rg804)*, as well as a mutation in *hmp-2*, did not cause any anal depressor defects (Fig. 5A).

WRM-1 and SYS-1 are involved in the regulation of daughter cell asymmetry during embryonic and larval cell division (Sawa and Korswagen, 2013). We used the RNAi-feeding method to knock down *sys-1* or *wrm-1* expression in developing L1 to adult males. RNAi of these genes individually induced major spicule developmental defects and interfered with normal anal depressor rearrangement (Fig. 5A,B). We then investigated whether *sys-1* and *wrm-1* are expressed in the anal depressor during rearrangement using direct protein fusions with mcherry and GFP, respectively (Baldwin and Phillips, 2014; Takeshita and Sawa, 2005). We did not find expression in the anal depressor, suggesting that β-catenin does not function in this cell. However, we did observe nuclear localization of SYS-1 in B.p after the first asymmetric B cell division in late L1 (Fig. 5C), suggesting this β-catenin is important in patterning the B cell descendants. Additionally, we observed WRM-1 expression and nuclear localization in the B.paa cell, which is produced through two divisions of B.p (Fig. 5D, Fig. S3I). Previous research established a role for *sys-1*, but not for *wrm-1*, in asymmetric B cell division (Wu and Herman, 2006). However, our observations suggest that these β-catenins could have roles in establishing cell differences during development.

Consistent with the idea that *sys-1* and *wrm-1* function in the B cell descendants and not the anal depressor, is the observation that the downstream effector of β-catenin TCF/LEF, encoded by *pop-1*, is not expressed in the anal depressor (Fig. 5E, Fig. S3F,G). Taken together, our results suggest SYS-1 and WRM-1 act with LIN-17 in the B cell descendants to promote anal depressor remodeling.

Calcium WNT pathways are involved in anal depressor rearrangement

We performed a mutant screen to identify additional signaling components that might participate with WNT-mediated remodeling. We exposed worms to ethyl methanesulfonate (EMS) and screened their progeny for sarcomere rearrangement defects that resemble the *egl-20(lf)* phenotype; consequently, we identified the mutant *rg441* (Fig. 6A). Using single-nucleotide polymorphism (SNP) mapping and whole-genome sequencing, we identified a nonsense mutation in the middle of PLC-β/*egl-8* (Fig. 6B) (Wicks et al., 2001; Lackner et al., 1999; Miller et al., 1999). PLC-β (phospholipase C-β) cleaves PIP_2 into IP_3 and DAG, resulting in Ca^{2+} release from the IP_3 receptor (Walker et al., 2009; Gower et al., 2005). Although PLC has not been shown to be associated with WNT signaling in *C. elegans*, it is downstream of WNT signaling in vertebrate systems (McQuate et al., 2017).

To determine whether *egl-8* acts with WNT signaling in the *C. elegans* male, we made a double mutant with the WNT ligand *egl-20*. The *egl-8* and *egl-20* mutants share additional phenotypes, including egg retention and the inability to sire progeny. If *egl-8* acts in an independent genetic pathway from *egl-20*, the severity of the double mutant phenotype should be greater than either single mutant. However, if they promote the same remodeling process, the

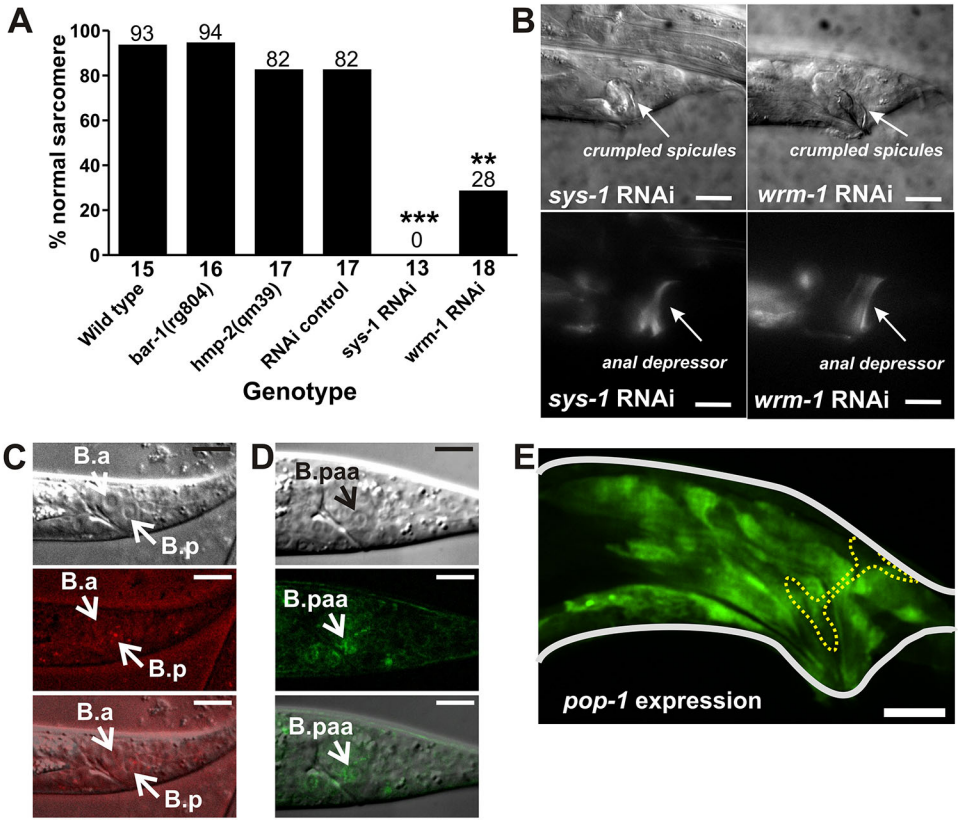

Fig. 5. β-Catenin functions in cells outside the anal depressor to regulate disassembly. (A) Graph depicting the percentage of males with normal sarcomeres (complete dorsal-ventral disassembly). Numbers above the bars indicate the percentage and the numbers below the *x*-axis represent the total sample number for each genotype. ***P*<0.005, ****P*<0.0001, Fisher's exact test. (B) DIC (top) and fluorescent (bottom) images of YFP:actin-expressing male tails developed in *sys-1* and *wrm-1* RNAi-expressing bacteria. Arrows indicate the spicules (DIC images) or the anal depressor (fluorescent images). (C) DIC (top) and fluorescent (middle) images of SYS-1:mcherry in the nucleus of B.p of a late L1 male. Bottom image is the top and middle images combined. Arrows indicate B.a and B.p. (D) DIC (top) and fluorescent (middle) images of WRM-1:GFP in the B.paa cell (arrow) of a L3 male. Bottom image is the top and middle images combined. (E) Fluorescent image of YFP expressed by the *pop-1* promoter. Adult male tail outlined in white. Anal depressor outlined by a yellow dashed line. Scale bars: 10 µm.

Development (2020) 147, dev181305. doi:10.1242/dev.181305

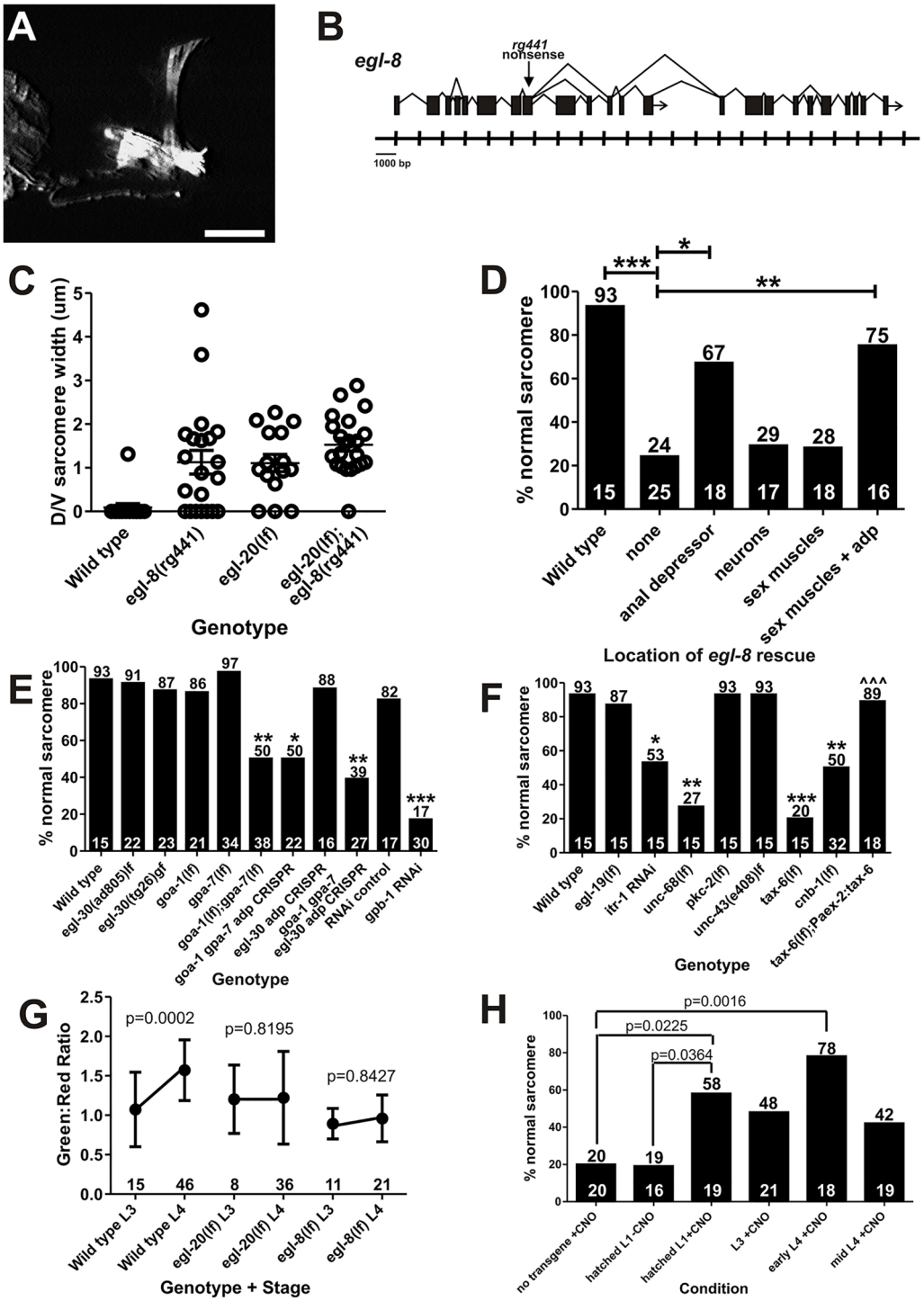

Fig. 6. PLC-β/EGL-8 promotes calcium release from internal stores to regulate anal depressor sarcomere disassembly. (A) Fluorescent image of *egl-8* mutant adult male anal depressor expressing YFP:actin. Dorsal is up and anterior is to the left. Scale bar: 10 µm. (B) Genomic structure and splice variants of *egl-8* with the location of the *rg441* allele in exon 8 indicated by the downward pointing arrow. Tick marks denote DNA base pairs in thousands. (C) Graph depicting the severity of disassembly defect. Each circle represents the dorsal-ventral sarcomere width of either the left or right dorsal attachment in one male. Data are mean±s.e.m. (D) Graph depicting the percentage (numbers on top of bars) of males with normal sarcomeres. The *x*-axis indicates where the wild-type *egl-8* minigene is expressed. adp, anal depressor. The numbers above the *x*-axis represent the total sample number for each location. **P*<0.05, ***P*<0.005, ****P*<0.0005, Fisher's exact test. (E,F) Graphs depicting the percentage (numbers on top of bars) of males with normal sarcomeres. The numbers above the *x*-axis represent the total sample number for each genotype/stage. **P*<0.05, ***P*<0.005, ****P*<0.0001, Fisher's exact test, compared with wild type. *itr-1* RNAi and *pkc-2(lf)* were scored using an P*unc-103*E:YFP:actin expressing transgene (Chen and García, 2015). (G) Calcium transients in the anal depressor monitored by measuring changes in G-CaMP fluorescence (green) normalized to an unchanging RFP control (red). Each dot indicates a time point where males were averaged±s.d. The *x*-axis represents genotype and developmental stage. The numbers above the *x*-axis represent the total sample number for each genotype/stage. *P*-values were determined using the Mann-Whitney *t*-test. (H) Percentage of adult ceDREADD-expressing *egl-20(lf)* males with a fully remodeled anal depressor. Males other than the 'no transgene +CNO' control have P*aex-2*::ceDREADD expressed from a transgene. *x*-axis indicates the developmental stage during which the males were first exposed to CNO. The numbers on top of the bars indicate the percentage of adult males with a normal sarcomere. The numbers above the *x*-axis indicate the total sample number for each condition. *P*-values were determined using Fisher's exact test.

Development (2020) 147, dev181305. doi:10.1242/dev.181305

double mutant phenotype should be similar to either single mutant. We found no statistical difference in the spectrum of sarcomere disassembly defects between single mutants and double mutants (Fig. 6C). This suggests that *egl-8* and *egl-20* participate in the same process. However, compared with the single mutants, fewer adult double mutant males had wild-type anal depressors (Fig. S4A). As EGL-8 has roles in other pathways, we do not rule out the possibility that EGL-8 also provides parallel WNT-independent contributions to anal depressor remodeling.

We next checked where PLC-β/*egl-8* functions to regulate sarcomere rearrangement. The *egl-8* expression pattern in *C. elegans* males includes the sex muscles, ray neurons, additional neurons in the tail and the anal depressor (Gower et al., 2005). We created an *egl-8* minigene using *egl-8* cDNA for exons 1-14 fused to genomic DNA for the remainder of the gene. Because the normal expression pattern of *egl-8* is determined by introns between exons 1-8 (Gower et al., 2005), we did not use its own promoter to drive expression. Instead, we used a series of tissue-specific promoters, including the *aex-2* promoter (anal depressor), the *rab-3* promoter (pan-neuronal), the *hlh-8* promoter [early M cell, from which sex muscles are descended (Harfe et al., 1998)] and the *unc-103E* promoter (sex muscles and anal depressor). We found that expressing *egl-8* in neurons or sex muscles did not rescue *egl-8(lf)* defects (Fig. 6D, Fig. S4B). However, expressing *egl-8* in either the sex muscles and anal depressor, or the anal depressor alone, rescued the sarcomere disassembly defects (Fig. 6D, Fig. S4B). Thus, EGL-8 functions in the anal depressor to regulate sarcomere disassembly during male development.

In *C. elegans*, *egl-8* is an effector of Gαq/EGL-30 (Xu and Chisholm, 2011; Lackner et al., 1999; Miller et al., 1999). We analyzed mutant males containing both loss- and gain-of-function mutations in *egl-30* and did not find any anal depressor defects (Fig. 6E). Thus, for anal depressor rearrangement, Gαq is either not required or functions redundantly with other Gα proteins.

We examined which other Gα proteins could be upstream of PLC-β. In the *Drosophila* WNT/Ca^{2+} pathway, the frizzled receptor is genetically upstream of Gαo (Katanaev et al., 2005). In *C. elegans*, Gαo is encoded by the broadly expressed *goa-1* (Mendel et al., 1995). Another possibility is *gpa-7*, a Gα present in the anal depressor (Hunt-Newbury et al., 2007). Similar to our *egl-30* mutant analysis, we did not find anal depressor defects in either *goa-1(lf)* or *gpa-7(lf)* single mutants (Fig. 6E). However, when we generated the *goa-1(lf); gpa-7(lf)* double mutant, we found that 50% of males had remodeling defects (Fig. 6E, Fig. S4C). In addition, some males also had an abnormal tail morphology (Fig. S4C). Thus, these Gα proteins redundantly promote anal depressor remodeling.

If the Gα proteins are functioning upstream of PLC-β/*egl-8*, they should also be functioning in the anal depressor. We attempted to address this issue by rescuing *goa-1* in the *goa-1(lf); gpa-7(lf)* strain but the double mutant produces too few viable progeny for maintaining transgenic lines. To address where these proteins function, we used tissue-specific CRISPR/Cas9. We designed guide RNAs to specific G-protein components and expressed Cas9 in the enteric muscles, using the *aex-2* promoter (Dickinson et al., 2013; Mahoney et al., 2008). We then expressed our tissue-specific CRISPR/Cas9 constructs in wild-type P*aex-2*:YFP:actin-expressing animals. Tissue-specific CRISPR/Cas9 should disrupt the gene only in the specific cells of interest. If males display mutant anal depressors, we can conclude that these cells use the wild-type genes for muscle remodeling.

We first checked whether our tissue-specific CRISPR/Cas9 Gα protein constructs were working by analyzing the *goa-1; gpa-7* combination. Similar in proportion to the genetic *goa-1(lf); gpa-7(lf)* double mutants, the *goa-1; gpa-7* anal depressor-targeted CRISPR/Cas9 animals displayed defective anal depressor remodeling (Fig. 6E), consistent with a cell-autonomous site of action. We then investigated whether *egl-30* might act redundantly with *goa-1* and *gpa-7* to promote remodeling. Triple mutants of *goa-1*, *gpa-7* and *egl-30* were not viable, so we generated *egl-30* single- and *goa-1; gpa-7; egl-30* triple tissue-specific CRISPR/Cas9 lines. However, we found that males containing *egl-30* single CRISPR/Cas9 transgenes were wild type, and males containing the guide RNAs to the three G-proteins had a phenotype that was no more severe than that in males containing tissue specific *goa-1; gpa-7* CRISPR/Cas9 transgenes (Fig. 6E). In contrast to the canonical pathway in other *C. elegans* tissues, there is a lack of evidence that Gαq/*egl-30* is upstream of PLC-β/*egl-8* signaling in male anal depressor remodeling (Xu and Chisholm, 2011; Lackner et al., 1999; Miller et al., 1999); this could be because of incomplete penetrance of the CRISPR constructs or because *egl-30* is not involved in the developmental process.

In addition to Gα proteins, PLC-β can be activated by the βγ subunits (Park et al., 1993). Using RNAi, we knocked down the expression of *C. elegans* Gβ *gpb-1* to examine whether perturbing other G protein members can disrupt anal depressor remodeling. Males grown with *gpb-1* RNAi were severely defective in terms of anal depressor remodeling during development (Fig. 6E, Fig. S4C). Therefore, functioning heterotrimeric complexes of Gβγ and GOA-1 or GPA-7 are needed to promote sarcomere disassembly.

The calcium released as a result of PLC-β/EGL-8 activation could come from internal or external stores. To determine the calcium source, we examined mutant worms defective in the cell membrane-located L-type voltage-gated Ca^{2+} channel EGL-19, and the ER-located IP_3 receptor ITR-1 and ryanodine receptor UNC-68 (Baylis et al., 1999; Lee et al., 1997; Maryon et al., 1996). We determined that, although the anal depressors of *egl-19(lf)* males appear normal, both *itr-1* RNAi and *unc-68(lf)* resulted in sarcomere disassembly defects (Fig. 6F, Fig. S4E). Thus, the calcium required for sarcomere disassembly is mobilized from internal stores.

WNT-promoted calcium release activates calcium-dependent kinases, including protein kinase C (PKC) and calcium/calmodulin-dependent kinase II (CaMKII) (Kuhl et al., 2000; Sheldahl et al., 1999; Slusarski et al., 1997). We examined the sarcomere structure in *C. elegans* males mutant in *pkc-2* (PKC) and *unc-43* (CaMKII), and determined that these effectors are not part of the remodeling pathway in the anal depressor (Fig. 6F, Fig. S4E).

Another known WNT effector is calcineurin, a calcium/calmodulin-dependent phosphatase that primarily works through NFAT (Ando et al., 2016; Saneyoshi et al., 2002). Although *C. elegans* does not have an NFAT homolog, the worm does have two genes that encode different calcineurin subunits: the phosphatase subunit *tax-6* and the regulatory subunit *cnb-1* (Bandyopadhyay et al., 2004; Kuhara et al., 2002). The *tax-6* gene is expressed in the anal depressor (Lee et al., 2005). We examined the anal depressor in males lacking either subunit and found that, in both cases, sarcomere rearrangement was impaired; this defect was rescued in *tax-6(lf)* males by enteric muscle-specific *tax-6* (Fig. 6F, Fig. S4E). Therefore, one effector for the increase in calcium in the anal depressor is calcineurin.

If increasing calcium signaling results in sarcomere rearrangement through WNT signaling, then removing WNT signaling should result in decreased calcium levels in the anal depressor. To measure this, we expressed the calcium-sensing fluorescent protein G-CaMP6 in the anal depressor of wild-type,

Development (2020) 147, dev181305. doi:10.1242/dev.181305

WNT/*egl-20(lf)* and PLC-β/*egl-8(lf)* mutant hermaphrodites and males (Correa et al., 2012; Tian et al., 2009; Nakai et al., 2001). We then recorded calcium changes from L2 to adult. Individual worms were placed on agar pads and the G-CaMP6 (calcium sensor) and RFP (control) fluorescent levels were measured at the developmental stage indicated (Fig. S4F,G, Fig. S5). Owing to the amount of data collected, we displayed the average and standard deviation for each sex and developmental stage (Fig. 6G, Fig. S4G). Calcium levels in the hermaphrodite anal depressor did not change during development (Fig. S4F,G). In contrast, the wild-type male showed an increase in calcium transients between L3 and L4, when rearrangement occurs (Fig. 6G, Fig. S4F,G), but not when the males were deficient in *egl-20(lf)* or *egl-8(lf)* (Fig. 6G, Fig. S5). These data support the idea that calcium release is correlated with muscle disassembly, and further indicate a role for WNT signaling through PLC-β.

Our experimental results suggest that WNT signaling works upstream of G-protein-coupled signaling to increase calcium levels in the anal depressor. Therefore, we investigated whether we could bypass the need for the WNT/EGL-20 ligand via artificially activating intracellular calcium signaling in the anal depressor. We used the *C. elegans* version of DREADD (ceDREADD), which is a modified *gar-3*-encoded G-protein-coupled receptor that is normally activated by acetylcholine. ceDREADD is stimulated by clozapine-N-oxide (CNO) (Prömel et al., 2016). The activated ceDREADD should promote intracellular calcium mobilization through signaling to PLC-β/EGL-8 but via Gαq/EGL-30 instead of GOA-1. We expressed ceDREADD in the anal depressor of *egl-20(lf)* mutant males using the *aex-2* promoter and then exposed these males to CNO to activate G-protein-driven signaling. Neither *egl-20(lf)* mutant males expressing ceDREADD without the CNO nor growing *egl-20(lf)* mutant males on CNO rescued the anal depressor defects (Fig. 6H). In contrast, when the ceDREADD-expressing *egl-20(lf)* males were placed on CNO plates at different time points, including hatched L1, L3, early L4 and mid L4, they developed normal adult anal depressors. ceDREADD-expressing males exposed to CNO as early L4s, when the anal depressor rearrangement begins, showed the largest developmental response to G-protein-driven calcium increase (Fig. 6H). Therefore, in wild-type males, the start of L4 is probably when the EGL-20/WNT ligand is activating G-protein-driven calcium increase to promote sarcomere disassembly.

DISCUSSION

Regulation of calcium levels is important in both development and disease progression (Paudel et al., 2018). There are different types of calcium signaling in muscle; one type is the brief spikes and subsequent calcium removal that control muscle contraction, and another is sustained calcium release that promotes longer-term changes. Altering the calcium handlers, which control the contractile machinery, can activate the pathways leading to changes in sarcomere structure and potential disease states (Shimizu et al., 2017). Here, we showed how and why a muscle activates sustained calcium release to disassemble a sarcomere (Fig. 7). Determining the regulation of these pathways is vital for addressing how to compensate for their dysfunction.

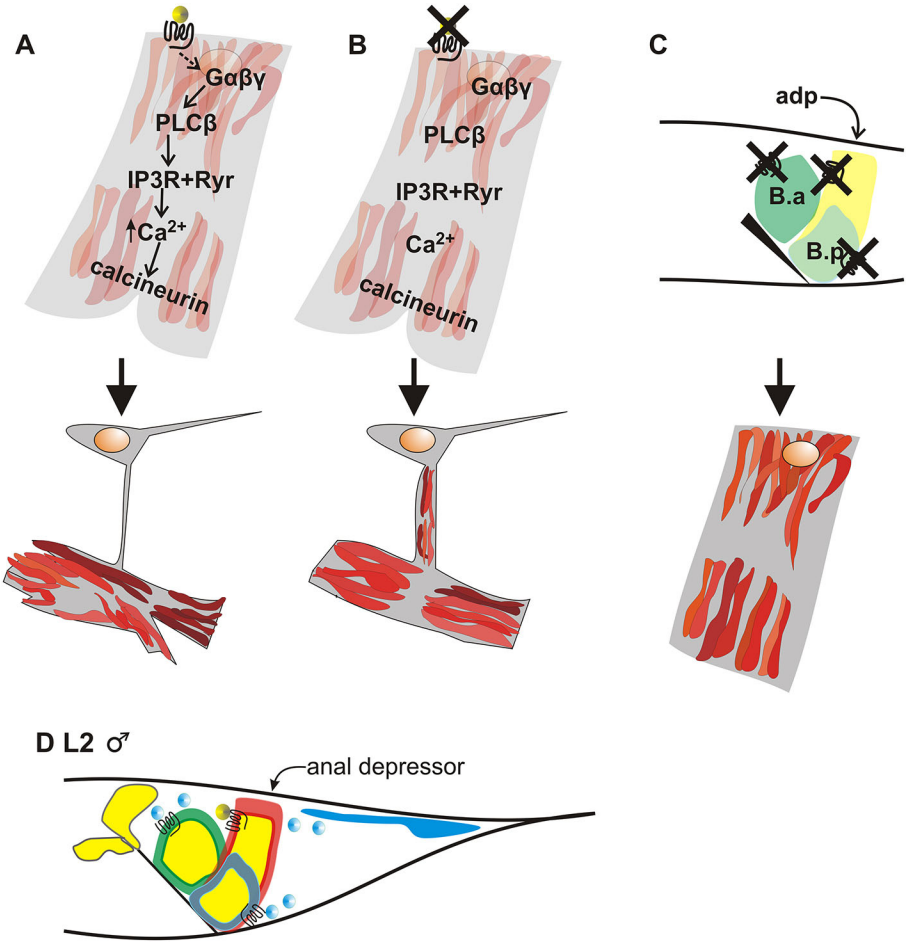

Fig. 7. A model for programmed muscle remodeling in the anal depressor. (A-C) Cartoon of cell signaling and anal depressor rearrangement. The outline of the cell is in gray. The actin component of the sarcomere is in red. The yellow circle is the WNT/EGL-20 ligand, which binds to the frizzled/LIN-17 receptor. The orange circle shows the location of the nucleus. (A) Wild-type anal depressor signaling and rearrangement. The top images represent early L4 stage and the bottom images represent the adult stage. (B) Inhibiting the WNT/Ca^{2+} pathway during development of the anal depressor results in incomplete sarcomere disassembly. (C) Inhibiting the WNT/Ca^{2+} pathway in the anal depressor (adp) and the WNT/PCP pathway of the surrounding epithelial B cell descendants (B.a and B.p) results in the adult male anal depressor resembling the larval muscle. The top image is of an L2 male tail. The black triangle depicts the anus. (D) Cartoon of an L2 male tail. adp, red outline; B.a cell, green outline; B.p cell, gray outline; WNT/LIN-44 ligand expression, blue; WNT/LIN-44 ligand, blue circles; WNT/EGL-20 expression, yellow; ligand itself, yellow circles; anus, black line.

Development (2020) 147, dev181305. doi:10.1242/dev.181305

Sustained calcium release can be a consequence of the WNT signaling pathway (McQuate et al., 2017). In the developing male anal depressor, sustained calcium release is accomplished through PLC-β (Fig. 7A). Similarly, in *C. elegans* adult wound closure, PLC-β is used to activate sustained calcium release, in this instance through a melastatin family (TRPM) channel and Gαq (Xu and Chisholm, 2011). Wound closure also requires cytoskeleton remodeling, indicating that sustained calcium release controlled by PLC-β is a preferred method to regulate programmed remodeling events.

Excitable cells need to separate sustained calcium release from the transient Ca^{2+} spikes, which are the basis for muscle contraction. In muscle, one enzyme known for responding to sustained but not transient calcium is the calcium/calmodulin-dependent serine/threonine phosphatase calcineurin (Dolmetsch et al., 1997). We showed that calcineurin is an important part of the signal transduction pathway activated by calcium levels in the anal depressor (Fig. 7A). Similar to our study, work in mice kidneys showed that calcineurin is activated via WNT signaling (independent of β-catenin), whereas CaMKII is not (Ando et al., 2016). Calcineurin has been reported downstream of WNT/Ca^{2+} signaling in other contexts, including promoting aquaporin localization to kidney cell membranes (Ando et al., 2016) and patterning in *Xenopus* embryos (Saneyoshi et al., 2002).

What the potential downstream targets of calcineurin are is an open question, as *C. elegans* lacks a common phosphatase target, the transcription factor NFAT (Graef et al., 2001). Known *C. elegans* targets of calcineurin include the transcription factor FOXO/*daf-16*, the transcriptional co-activator CRTC-1 and a gene of unknown function, *cnp-1* (Tao et al., 2013; Jee et al., 2012; Mair et al., 2011). However, whether these potential targets are expressed in the anal depressor is not known. Remodeling events often include transcription regulation, therefore calcineurin targets might include molecules that regulate transcription. Additionally, CRTC-1 is important in monitoring energy status, and *C. elegans* might find linking the high-energy-demand remodeling process with the energy status of the organism beneficial (Burkewitz et al., 2015).

Calcineurin is also activated in response to elevated calcium levels that lead to the removal of excess neuronal synapses during development (Miller-Fleming et al., 2016). This removal might be dependent on a member of the cell death pathway, *ced-4*, which activates a protein that cleaves F-actin (Meng et al., 2015). Although these studies focused on neurons, *C. elegans* muscle might use a similar mechanism for cytoskeletal remodeling. The effectors of calcineurin in the anal depressor could include molecules involved in the disassembly process and/or transcription-associated genes that regulate genes that participate in remodeling.

Mutating components of the WNT/Ca^{2+} pathway in the anal depressor results in males with adult sarcomeres that were only partially disassembled during development (Fig. 7B). However, mutating components of the WNT pathway in the surrounding epithelial cells (the B cell descendants) along with components in the anal depressor results in a complete lack of larval sarcomere disassembly (Fig. 7C). Noncanonical WNT/PCP signaling is important for determining anterior-posterior cell identity, as the B cell descendants go through several rounds of asymmetrical divisions (Wu and Herman, 2006; Sulston et al., 1980). In this paper, we also show a role for β-catenin-like proteins WRM-1 and SYS-1 in B cell descendant patterning. We propose that these cell divisions result in epithelial progeny that the anal depressor uses as instructors for its rearrangement. Although the anal depressor does not rearrange until the male reaches the L4 developmental stage, the male anal depressor probably receives competence information from the B cell descendants before remodeling occurs (Fig. 7D) (Chen and García, 2015).

Drastic muscle remodeling is found in humans in disease states, such as pathological heart muscle remodeling following cardiac damage (Parra and Rothermel, 2017). These pathological models show similar molecular mechanisms to those identified in the *C. elegans* anal depressor. However, the anal depressor presents an advantage, as this is not a pathological state, but a normal deterministic program. We are able to discover how these pathways function under normal biological conditions, which can provide insight into how they are co-opted to produce disease states. Separately, WNT and calcineurin signaling are known to be involved in the pathological cardiac remodeling that takes place following injury, although these two signaling pathways are rarely explicitly linked in this context (Fu et al., 2019; Parra and Rothermel, 2017; Freire et al., 2014; Yoshida et al., 2004). Our work demonstrates a direct link between WNT and calcineurin signaling in programmed muscle remodeling, highlighting the need to focus on how these pathways integrate to coordinate this process. Furthermore, the calcineurin effector NFAT seems to be primarily involved in the pathological response to increased calcium signaling following cardiac injury, whereas the effectors activated as a result of physiological responses remain unknown (Zhao et al., 2019; Parra and Rothermel, 2017; Balakumar and Jagadeesh, 2010). As *C. elegans* does not have an NFAT homolog, and we are studying a non-pathological remodeling event, this system provides a unique opportunity to determine additional calcineurin targets, thereby separating pathological and physiological responses.

MATERIALS AND METHODS

Experimental model and subject details

Caenorhabditis elegans and bacterial strains

C. elegans strains were cultured at 20°C and manipulated following standard protocols (Brenner, 1974). Strains listed as 'Wild type' contained *him-5(e1490)* on LG V (Hodgkin et al., 1979). Bacteria strains used to feed worms include *Escherichia coli* OP50 for nearly all experiments and HT115(DE3) for RNAi experiments.

The *egl-8(rg441)* allele described in this study was isolated from an EMS screen that selected for males that have anal depressor sarcomere disassembly defects. The strain CG941, which carries the integrated transgene *rg*Is*3* [P*lev-11*:RFP; P*lev-11*:G-CaMP], was mutagenized to generate mutant lines. The *rg441* strain was identified and outcrossed four times to eliminate background mutations. Whole-genome sequencing was conducted by BGI Americas Corporation, in combination with SNP mapping (Wicks et al., 2001), to locate the *rg441* allele within the *egl-8* locus on LG V. The *rg441* mutation changed the wild-type sequence CTTGACCAAT to the mutant sequence CTTGACTAAT (Gln to Ochre).

The *bar-1(rg804)* allele described in this study was isolated using CRISPR/Cas9 as described by Dickinson et al. (2013). Plasmid construction is described below. Additional alleles and strains, as well as primers, resources and reagents, used in this study are listed in Table S1.

Method details

Plasmid construction, transgenic strain and integrated line generation

Construction of P*aex-2*:YFP:actin integration

We removed the introns from the genomic actin sequence with YFP fused at the N terminus that we used previously in Guo et al. (2012) and Chen and García (2015) to create the plasmid pXC22. This plasmid contained an Invitrogen Gateway Reading Frame Cassette (RfC), allowing for recombination with pBL348 [plasmid contains the *aex-2* promoter (LeBoeuf and Garcia, 2017)] to create pBL397. pBL397 was injected with pLR361(Pges-1:RFP) and pUC18 into N2 hermaphrodites. The *ges-1* promoter drives expression in the intestine and we used it as a marker for the generation of transgenic lines (Egan et al., 1995). A transgenic line was

Development (2020) 147, dev181305. doi:10.1242/dev.181305

selected for UV-irradiation-based integration (Mello and Fire, 1995) to create strain CG1640 that contains the *rg*Is*15* integration. *rg*Is*15* was mapped to LGX. This integration was then combined with other mutations to visualize anal depressor sarcomere morphology. 'Wild type' in this paper refers to strain CG1722, which is the *rg*Is*15* integration with the *him-5(e1490)* mutation.

Nearly all strains in which the anal depressor sarcomere was visualized contain *rg*Is*15*. A few strains, indicated when used, contain a transgene with Punc-103E:YFP:genomic actin, which was created as described by Chen and García (2015).

Construction of P*aex-2*:YFP integration

The plasmid containing P*aex-2* (pBL348) was recombined with pGW77YFP, which contains an RfC and YFP to generate pBL351. pBL351 was injected with pLR361(P*ges-1*:RFP) and pUC18 into N2 hermaphrodites. A transgenic line was selected for UV-irradiation-based integration to create strain CG1647 that contains the *rg*Is*21* integration. *rg*Is*21* was mapped to LGII. This integration was then combined with other mutations to visualize anal depressor morphology.

Construction of *lin-17* cDNA plasmids

The full length *lin-17* cDNA was PCR-amplified using primers flin-17 and lin-17r. This PCR product was ligated to linearized pBL405 (see section on construction of *egl-20* plasmids for further details) using Takara Bio In-Fusion (linearizing primers: DownRmvsdha and UPremegl20) to create pBL423. This plasmid was sequenced and a point mutation was fixed using primers fpBL423a and pBL423ar to create pBL426. pBL426 was recombined with pBL348 (P*aex-2*), pXC11 (P*lin-17*) and pLR21 (P*unc-103E*) (Reiner et al., 2006) to create pBL428, pBL429 and pBL427, respectively. pXC11 was created using primers attB1-Plin-17-Forward and attb2-Plin-17-Reverse to amplify the 6.5 kb region upstream of the *lin-17* ATG from genomic DNA, and then recombining that PCR product with pDG15 (Reiner et al., 2006). pXC11 was recombined with pGW322YFP to create pXC12 (Plin-17:YFP). The RFP in pBL426 was replaced with cyan fluorescent protein (CFP) using primers fpBL412CFP and pBL412CFPr to amplify CFP, and fpBL412 and pBL412r to linearize pBL426 minus RFP. An In-Fusion reaction combined the two PCR products to create pBL444. pBL444 was recombined with pBL455 (P*pop-1*) to create pBL457. pBL455 was created using primers FPpop-1 and Ppop-1R to amplify the 2.6 kb region upstream of the *pop-1* ATG from genomic DNA and then recombining that PCR product with pDG15. pBL427, pBL428, pBL429 and pBL457 were injected with pUC18 and pBX1 (*pha-1*) (Schnabel and Schnabel, 1990) as a marker for transgenic lines into the strain CG1721.

The *pop-1* promoter expression pattern in males was determined by recombining pBL455 with pGW77YFP to create pBL462. This plasmid was injected into CG531 males with pBX1 and pUC18 to create CG1753.

Construction of *lin-44* genomic plasmids

Genomic *lin-44* DNA was PCR amplified using primers RVL44gnmJG44lnks and FL44pxc99lnks. This PCR product was ligated to linearized pBL405 using Takara Bio In-Fusion to create pBL407. pBL407 was recombined with pXC108 (P*lin-44*) to create pBL409. pXC108 was created using primers Flin-44pro and lin-44proR to amplify the 2.7 kb region upstream of the *lin-44* ATG from genomic DNA and then recombining that PCR product with pDG15. pBL409 was injected with pUC18 and P*myo-2*:GFP as a marker for transgenic lines into the strain CG1692.

Construction of *egl-20* plasmids

Genomic *egl-20* sequence (2.3 kb) from ATG to the last stop codon was PCR amplified using the primers egl-20-coding-F and egl-20-coding-R. These two primers contain homology to the sequences that flank the G-CaMP3-coding sequence in pLR279. The primers linear-pLR306-formab-5-for and linear-pLR306-formab-5re were used to linearize pLR279 and remove the G-CaMP-coding sequence. The two primers contain homology to the 3′ and 5′ sequence of the *egl-20* genomic sequence, respectively. The *egl-20* genomic sequence was ligated into the SL2:DsRed plasmid backbone using In-Fusion to make pXC99 (the gateway *ccdB* cassette: *egl-20*:SL2:RFP). A loxP site was added in front of the *egl-20* ATG using primers UpForloxPegl20 and RevLOXPegl20 to PCR amplify pXC99. The primers contain the loxP site; after amplification, the original plasmid was removed by DpnI digestion, leaving only the amplified plasmid with loxP sites, which was ligated using NEB Quick Ligase. This process created plasmid pBL404. The process was repeated using primers Fordwnxc99loxP and Revdwnxc99loxP to add loxP sites after RFP to create plasmid pBL405.

We then added the *egl-20* 3′UTR to the plasmid. The plasmid itself was amplified using primers fpBL405sl2 and pBL405egl-20r. The *egl-20* 3′UTR was amplified using primers Fegl-20 3′UTR and Egl-20 3′UTRr. These PCR products were ligated together using In-Fusion to create plasmid pBL412 (RfC:loxP:*egl-20*:3′UTR:SL2:RFP:loxP). This plasmid was recombined with pXC33 (P*egl-20*), pBL348 (P*aex-2*) and pXC108 (P*lin-44*) to create pBL415, pBL416 and pBL422, respectively. These plasmids were injected along with pUC18 and P*myo-2*:GFP into the strain CG1673 to generate transgenic lines.

pXC33 contains the 7 kb promoter region of *egl-20* and was cloned using primers Pegl-20-For-1 and Pegl-20-Re-1-imme-beforeATG recombined with pDG15 (Whangbo and Kenyon, 1999). We created a plasmid to determine *egl-20* expression in males by recombining pXC33 with pLR186 (RfC:DsRed1-E5) (LeBoeuf et al., 2011) to make pXC35. pXC35 was injected into *him-5(e1490)* hermaphrodites with P*myo-2*:GFP as an injection marker. A transgenic line was selected for UV-irradiation-based integration to create strain CG1656 that contains the *rg*Is*23* integration. *rg*Is*23* was mapped to LGV. This integration was then used to visualize *egl-20* expression patterns in males.

We replaced the RFP in pBL412 with CFP using primers fPBL412 and pBL412r to amplify pBL412 without RFP, and amplified CFP using primers fpBL412CFP and pBL412CFPr. We ligated the two PCR products together using In-Fusion to create plasmid pBL436. pBL426 was recombined with pBL455 (P*pop-1*) to create plasmid pBL476. pBL476 was injected with pUC18 and Pmyo-1:GFP into the strain CG1673 to generate the transgenic line CG1762.

Genomic *egl-20* sequence (2.3 kb) from ATG to the codon before the stop codon was PCR-amplified using primers Fegl-20pPD122 and egl-20pPD122R. The primers contained homology for pPD122-39, which contains two transmembrane domains from *pat-3* integrin tagged with YFP (Gettner et al., 1995). pPD122-39 was amplified using primers FpPD122-39 and pPD122-39R. The two PCR products were combined using In-Fusion to create plasmid pBL481. We then added a Gateway Reading Frame Cassette (RfC) to pBL481 using primers pBL481f and RpBL481 to amplify the plasmid and primers ForRfC and RfcRev to amplify the RfC. We ligated the two PCR products together to create plasmid pBL484, which we recombined with pBL455 (P*pop-1*) and pBL348 (P*aex-2*) to create pBL486 and pBL487. pBL486 and pBL487 were injected along with pUC18 and P*myo-2*:GFP into strain CG1652 to create strains CG1812 and CG1801, respectively.

Construction of the *egl-8* minigene

Owing to the size of the *egl-8* locus (23 kb), a minigene was created. Primers Fegl-8atg and egl-8midR were used to PCR amplify the first half of the *egl-8* cDNA. This product was ligated to plasmid pBL405 (ccdB:loxP:*egl-20*:SL2:RFP:loxP) that had been linearized using primers DownRmvsdha and UPremegl20 to remove *egl-20* and add *egl-8* in its place using an In-Fusion Dry-Down PCR Cloning Kit to create plasmid pBL424. Next, the second half of the *egl-8* cDNA was amplified from pXC78, which contains *egl-8* genomic sequences. pXC78 was constructed using primers e8-12-16ex-2nd-for and e8-12-16ex-2nd-re to amplify the *egl-8* genomic region from exon 12 to exon 16. This PCR product was recombined with pDG15 using BP clonase to make pXC53. We then cloned the genomic region from exon 17 to the genomic sequence that is 3.6 kb downstream of *egl-8* using the primers egl-8-17th-down-for and egl-8-17th-down-re. The primers contain homology to the 3′ end of exon 16. pXC53 was linearized using primers lin-e8-12-16pdg15-f17-d-for and lin-e8-12-16pdg15-f17-d-re. The PCR product of exon 17 to the downstream sequence was ligated into pXC53 using In-Fusion to make pXC54 (*egl-8* genomic sequence from exon 12 to the 3.6 kb sequence downstream of *egl-8*). The insertion mutation contained

Development (2020) 147, dev181305. doi:10.1242/dev.181305

within pXC54 was corrected by single-site mutagenesis to make pXC78 (*egl-8* genomic sequence from exon 12 to the 3.6 kb sequence downstream of *egl-8* with the mutation corrected).

From pXC78, *egl-8* was PCR-amplified using primers Fegl-8exon14 and Egl-8 3UTR. This was ligated using an In-Fusion reaction with linearized pBL424, linearized using primers DownRmvsdha and pBL424r, to create plasmid pBL425. pBL425 was sequenced, revealing two point mutations in the genomic region of *egl-8*. These two mutations were fixed using primers (Finfegl-8ex14 and Infegl-8ex17R) that did not contain the point mutations to amplify a PCR product that was then ligated using In-Fusion to pBL425 linearized using primers pBL425egl-8r and FpBL425egl-8 to create plasmid pBL432. pBL432 was sequenced and found to contain a mutation in one exon. This mutation was fixed by amplifying the area containing it with the primers FEgl-8exon15a and egl-8exon20R and then combined using In-Fusion with a linearized pBL432 using primers FEgl-8mini and egl-8miniR to create pBL447. pBL447 contains the *egl-8* minigene with no mutations.

To create *egl-8* expression constructs, pBL447 was recombined using LR Clonase with pBL348 (P*aex-2*), pBL363 [P*rab-3* (LeBoeuf and Garcia, 2017)] and pBL458 [P*unc-103E* (smaller version)] to create plasmids pBL448, pBL449 and pBL459, respectively. These plasmids were injected along with pUC18 and P*myo-2*:GFP into the strain CG1697 to create transgenic lines.

pBL458 contains a shorter version of P*unc-103E* that was originally published by Reiner et al. (2006). The original P*unc-103E*, at 5.4 kb, was deemed too large to work with the 16.2 kb pBL447. Since the publication by Reiner et al. (2006), another *unc-103* exon 1 was identified within the original P*unc-103E* (LeBoeuf and Garcia, 2017). This exon and promoter were removed to create a shorter version (2.4 kb) of P*unc-103E* using primers FPunc-103E-J and Punc-103E-JR. This promoter was recombined with pDONR using BP clonase to create pBL458.

As the *hlh-8* promoter is too large to put in front of the *egl-8* minigene, the pXC27 plasmid (Chen and García, 2015) containing P*hlh-8* was co-injected with pBL447. Functional transgenes were confirmed by fluorescent imaging of the RFP tag.

Construction of the *tax-6* genomic DNA plasmid

The full-length genomic DNA of *tax-6* was PCR amplified from purified *C. elegans* genomic DNA using primers Ftax-6lowcopy and tax-6R. In-Fusion was used to combine this PCR product with pBL436 linearized with primers FCFPATG and RpBL436wRfCB to create plasmid pWD5(RfC:*tax-6*:CFP). There were two mutations in *tax-6*, one in exon 6 and one in exon 11. We used primers that fixed these mutations, Ftax-6ex6 and tax-6ex11R, to create a 3665 bp PCR product. We used primers FpWD5 and pWD5R to amplify the rest of the plasmid. We then used In-Fusion to put these two PCR products together, creating plasmid pBL498(RfC:tax-6:CFP). We used LR Clonase to recombine this plasmid with pBL348(Paex-2) to generate plasmid pBL499.

Construction of P*aex-2*:G-CaMP6M:SL2:RFP integration

To reliably measure differences in calcium levels in the anal depressor across strains, we generated a G-CaMP integrated line. We injected pBL352 (P*aex-2*:G-CaMP6M:SL2:RFP) (LeBoeuf and Garcia, 2017) into N2 with P*acr-10*:YFP as an injection marker. A transgenic line was selected for UV irradiation-based integration to create strain CG1644 that contains the *rg*Is*19* integration. *rg*Is*19* was mapped to LGII. This integration was then used to visualize calcium levels in the anal depressor in *egl-20* and control males.

DREAD expression

The *C. elegans* designer receptors exclusively activated by designer drugs (*ce*DREADD) has been described previously and extensively characterized by Prömel et al. (2016). In short, the muscarinic G-protein sequence of *gar-3*:YFP in the plasmid pLR344 contains Y146C and A237G substitutions, which make the expressed G-protein-coupled receptor insensitive to acetylcholine but sensitive to clozapine-N-oxide (CNO). The *aex-2* promoter from the plasmid pBL348 was recombined in front of the *ce*DREADD sequence using LR clonase, to make the plasmid pLR345.

P*aex-2*:ceDREADD::YFP was introduced into *C. elegans* by injecting 20 ng/µl pLR348, 20 ng/µl pPD132.102 (P*myo-2*:GFP) and 160 ng/µl of pUC18 into the germline of CG1673 hermaphrodites to generate the extrachromosomal array *rg*Ex841 in strain CG1806.

The DREADD ligand CNO (Sigma-Aldrich) was dissolved in dimethyl sulfoxide (DMSO) to make a 20 mM stock solution. The CNO stock solution was further diluted in M9 buffer and added to NGM plates, so that the final drug concentration in the plates was 100 µM. OP50 was then spotted onto the CNO-containing plates and allowed to grow overnight. The next day, five or six CG1806 hermaphrodites were placed on the CNO- or DMSO blank-plates. The anal depressor of their transgenic adult male progeny was then analyzed by microscopy. L3, early L4 and mid L4 CG1806 males grown under normal conditions (without CNO) were identified and transferred to CNO plates. Their anal depressors were analyzed by microscopy once they were adults.

bar-1 plasmid construction

We generated a CRISPR/Cas9 plasmid targeting *bar-1* using primers bar-1sgRNA1 and sgRNA-Rev-common to create pBL468. We injected pBL468 into CG1640, isolating CG1780. We sequenced CG1780 and determined that in the sequence 5′ CACCGCAAGGTGG the four underlined bases were deleted. TGG in the sequence is the PAM site we chose, indicating the Cas9 enzyme cut exactly where it was designed to.

The 6.3 kb promoter region of *bar-1* was cloned using the primers bar-1-promot-F and bar-1-promot-R. The primer set contains the ATTB site, therefore the promoter region was recombined, using BP clonase, into pDG15 to generate pXC67. pXC67 was recombined with pGW322YFP to make pXC70 (P*bar-1*:YFP). The genomic sequence of *bar-1* from ATG to codon 761 was PCR-amplified using the primers bar1-coding-F and bar1-coding-R. The primers contain homology to the 3′ end of bar-1 promoter region and 5′ end of YFP. pXC70 (P*bar-1*:YFP) was linearized using primers linPbY-For2nd-infbar1-761 and lin-PbY-infcod-R. The primer set contains homology to the 3′ end and 5′ end of cloned *bar-1* genomic sequence, respectively. The *bar-1* genomic region was infused with the linearized vector pXC70 using In-Fusion to make pXC87 (P*bar-1*:bar-1:YFP). pXC67 (P*bar-1*) was also recombined with pGW77C (plasmid containing Gateway ATTR site in front of CFP) to make pXC93 (P*bar-1*:CFP). pXC93 and pXC87 were injected with pBX1 and pUC18 into CG531 to make CG1572.

RNAi

itr-1

rrf-3(pk1426); him-5(e1490) L4 hermaphrodites carrying the transgene *rg*Ex*497* (P*unc-103E*: YFP::actin) were fed with bacteria producing double-stranded RNAs to target the open reading frame of *itr-1*. Bacteria with the L4440 (control) or double-T7 vector including exons of target genes were grown and induced by isopropylthio-β-D-galactoside (IPTG) using a standard protocol (Kamath et al., 2001). Carbenicillin was used at the concentration of 10 mg/ml to increase the level of plasmid maintenance and therefore the effectiveness of RNAi. Exons 14 to 19 of *itr-1* were cloned into the double-T7 vector. Males that displayed the corresponding mutant phenotype were picked for anal depressor imaging and defects detection.

wrm-1 and *sys-1*

The Gateway ATTP sequence was PCR-amplified from the Gateway entry vector pDONR221 (Invitrogen) and inserted in the NheI site, between the double T7 promoters of the L4440 vector (Addgene), to generate the plasmid pMB3. Fragments (300-400 bp) of *sys-1* and *wrm-1* exon 3 were PCR amplified with the primer pairs: Attb1sys1, Attb2sys1, and Attb1wrm1, Attb2wrm1, respectively. The PCR fragments were recombined into pMB3 using BP clonase (Invitrogen) to generate the plasmids pLR390 (*sys-1* RNAi) and pLR391 (*wrm-1* RNAi). pLR390 and pLR391 were transformed into the T7 RNA polymerase-expressing strain HT115(DE3).

A drop of solution containing four parts bleach and three parts 4 N NaOH was added to groups of gravid *rgIs*15 hermaphrodites that were placed on bacteria-free NG plates. The lack of food stalled the development of L1 worms that hatched from the bleach-resistant eggs. The next day, HT115(DE3) cells

Development (2020) 147, dev181305. doi:10.1242/dev.181305

containing pLR390 or pLR391 were grown in a shaking incubator at 37°C in Luria-Bertani broth containing 100 µg/ml of carbenicillin. When the bacterial culture reached mid-log density, IPTG was added at a final concentration of 100 µM. Cells were grown for an additional hour, centrifuged for 5 min at 21,000 ***g***, concentrated 10× and spotted on a nematode growth (NG) plate that contained 100 µg/ml of carbenicillin and 100 µM IPTG. The overnight-synchronized starved L1 animals were then added to the HT115(DE3)-containing plates. Adult males were scored using fluorescence microscopy.

CRISPR/Cas9-mediated disruption of *goa-1*, *gpa-7*, *egl-30* and *gpb-1* in the anal depressor

We replaced the *eft-3* promoter, which drives Cas9 in pDD162 [the Cas9-expressing empty sgRNA plasmid (Dickinson et al., 2013)], with the Gateway *ccd*B destination cassette A (Invitrogen) to generate pYW42. To drive Cas9 expression in the anal depressor, LR clonase (Invitrogen) was used to recombine the *aex-2* promoter from pBL348 into pYW42 to generate pLR392. To generate the *goa-1* CRISPR/Cas9 guide RNA plasmid pLR393, the 19 base pair guide sequence to exon 2 of *goa-1* (5′ AGCCATGAGCAACTTAGGC 3′) was added to pLR392 using PCR and the primers goa1gRNA and sgRNA(universal)REV. To generate the *gpb-1* CRISPR/Cas9 guide RNA plasmid pLR394, the 19 bp guide sequence to exon 8 of *gpb-1* (5′ GGCTGGTCACGATAACCGA 3′) was added to pLR392 using PCR and the primers gpb1gRNA and sgRNA(universal)REV. To generate the *gpa-7* CRISPR/Cas9 guide RNA plasmid pLR397, the 19 base pair guide sequence to exon 3 of *gpa-7* (5′ AGCGTGACTCCCAGTTAGT 3′) was added to pLR392 using PCR and the primers Gpa7gRNA and sgRNA(universal)REV. To generate the *egl-30* CRISPR/Cas9 guide RNA plasmid pLR400, the 19 base pairs guide sequence to exon 2 of *egl-30* (5′ GACTTGTCTATCAGAACGT 3′) was added to pLR392 using PCR and the primers Egl30gRNA and sgRNA(universal)REV.

Injection mixes containing: 160 ng/µl pUC18, 20 ng/µl pBL65 (P*ges-1*::CFP) and 20 ng/µl pLR394 (P*aex-2*:Cas9; *gpb-1* gRNA); 160 ng/µl pUC18, 20 ng/µl pBL65 and 20 ng/µl pLR400 (P*aex-2*:Cas9; *egl-30* gRNA); 140 ng/µl pUC18, 20 ng/µl pBL65 and 20 ng/µl each of pLR393 (P*aex-2*:Cas9; *goa-1* gRNA) and pLR397 (P*aex-2*:Cas9; *gpa-7* gRNA); or 120 ng/µl pUC18, 20 ng/µl pBL65 (P*ges-1*::CFP) and 20 ng/µl each of pLR395, pLR397 and pLR400 were microinjected into the germline of *rgIs*15 hermaphrodites.

The anal depressors of transgenic males, which express the co-injected P*ges-1*::CFP in the intestine, were scored using fluorescence microscopy. Transgenic males, which contain pLR394 (P*aex-2*:Cas9; *gpb-1*gRNA) and died as L1 larvae, were constipated or were obviously mosaic for the transgene and superficially wild type; transgenic males that were constipated at L1 to L3 larval stages were picked for inspection. Transgenic males that contain either P*aex-2*:Cas9; *egl-30* gRNA or P*aex-2*:Cas9; *goa-1*, gpa-7 gRNA or P*aex-2*:Cas9; *goa-1*, *gpa-7* and *egl-30* gRNA, transmit the extrachromosomal array well; all adult males that expressed a CFP-fluorescent intestine were inspected.

Imaging and measurements

To facilitate imaging, the worms were mounted on agar pads made from a melted agar solution (Sulston and Horvitz, 1977). The agar solution was made by adding M9 to Difco Noble agar. The concentration of the agar pads for larval males and hermaphrodites was 2%. We used abamectin (Sigma-Aldrich) to immobilize the worms without interfering with development. Treatments such as NaN_3, levamisole, arecoline, nicotine and dopamine killed the worms, wore off after a period of time or stalled development. Abamectin opens glutamate-gated chloride channels, which are located on the ventral cord neurons, leading to paralysis (Hart et al., 1995; Maricq et al., 1995). However, the larval anal depressor does not seem to have abamectin-sensitive receptors. We made a stock of 50 mg/ml in DMSO and then added 5 µl of stock solution to 1 ml of M9. This solution was then used to pick the worms via a glass needle from the plates they were grown on. After a few minutes, the worms were paralyzed and transferred to the agar pads. This same procedure was used for adult males, as abamectin did not change the structure of the tail, allowing for clear visualization of tail structures. Cover slips were then put on the top of the worm. All the images were taken using an Olympus IX81 microscope fitted with a Yokogawa CSU-X1 Spinning Disk Unit (Andor Technology). The two outermost lateral sides of the worm tail were set up as the starting and ending *z* stack for optical sectioning. Series of confocal images were then collected from one lateral side of the worm tail to the other. For each animal, the image that best showed the dorsal-ventral sarcomere width was selected. If no single image gave a good area for measurement, images of the individual attachment (either the left or the right) of the anal depressor were overlaid together using MetaMorph software (version 7.8.0.0, Molecular Devices) to create a flattened image. A line that had been calibrated for the magnification used was then drawn to determine the dorsal-ventral sarcomere width.

Calcium imaging

Males at the mid-L4 stage were placed on agar pads that were made from 2.5% noble agar dissolved in S-basal solution. Abamectin was added to the agar solution to immobilize the worm. The final concentration was 0.25 mg/ml. The G-CaMP and DsRed fluorescence signals at the male tail were recorded simultaneously using a dual view simultaneous image splitter (Photometrics) and a Hamamatsu ImagEM Electron multiplier (EM) CCD camera, with an exposure time of 1 s. The worms were imaged using the 40× objective, and the imaging continued until the worm reached the L4-molt stage. The Ca^{2+} data were analyzed using the Hamamatsu SimplePCI (version 6.6.0.0) software and Microsoft Excel, as previously described (LeBoeuf et al., 2011).

Cell ablations

CG1722 L2 or L3 males were mounted on 2% noble agar pads dissolved in M9 plus 12 mM NaN_3. Cell ablations were performed as described by Bargmann and Avery (1995) using a Micropoint 337-NDS-USAS laser (Photonic Instruments) attached to an Olympus BX51 microscope.

Quantification and statistical analysis

Graphs and statistical analysis were constructed and carried out using GraphPad Prism 5.

Acknowledgements

We thank the *Caenorhabditis* Genetics Center for providing strains [funded by the National Institutes of Health Office of Research Infrastructure Programs (P40 OD010440)]; Bryan Phillips for the BTP105 strain; and Kyoungsun Rha, Jimmy Goncalves, Yufeng Wan, Paola Correa, Liusou Zhang, Changhoon Jee and Daisy Gualberto for discussion and manuscript review.

Competing interests

The authors declare no competing or financial interests.

Author contributions

Conceptualization: B.L., X.C., L.R.G.; Methodology: B.L., X.C., L.R.G.; Validation: B.L., X.C., L.R.G.; Formal analysis: B.L., X.C., L.R.G.; Investigation: B.L., X.C., L.R.G.; Resources: B.L., X.C., L.R.G.; Writing - original draft: B.L.; Writing - review & editing: X.C., L.R.G.; Visualization: B.L., X.C., L.R.G.; Project administration: L.R.G.; Funding acquisition: L.R.G.

Funding

This work was supported by a gift from the Howard Hughes Medical Institute awarded to L.R.G.

Supplementary information

Supplementary information available online at
http://dev.biologists.org/lookup/doi/10.1242/dev.181305.supplemental

References

Alexandre, C., Baena-Lopez, A. and Vincent, J.-P. (2014). Patterning and growth control by membrane-tethered Wingless. *Nature* **505**, 180-185. doi:10.1038/nature12879

Ando, F., Sohara, E., Morimoto, T., Yui, N., Nomura, N., Kikuchi, E., Takahashi, D., Mori, T., Vandewalle, A., Rai, T. et al. (2016). Wnt5a induces renal AQP2 expression by activating calcineurin signalling pathway. *Nat. Commun.* **7**, 13636. doi:10.1038/ncomms13636

Balakumar, P. and Jagadeesh, G. (2010). Multifarious molecular signaling cascades of cardiac hypertrophy: can the muddy waters be cleared? *Pharmacol. Res.* **62**, 365-383. doi:10.1016/j.phrs.2010.07.003

Baldwin, A. T. and Phillips, B. T. (2014). The tumor suppressor APC differentially regulates multiple β-catenins through the function of axin and CKIα during *C. elegans* asymmetric stem cell divisions. *J. Cell Sci.* **127**, 2771-2781. doi:10.1242/jcs.146514

Bandyopadhyay, J., Lee, J. and Bandyopadhyay, A. (2004). Regulation of calcineurin, a calcium/calmodulin-dependent protein phosphatase, in *C. elegans*. *Mol. Cells* **18**, 10-16.

Bargmann, C. I. and Avery, L. (1995). Laser killing of cells in *Caenorhabditis elegans*. *Methods Cell Biol.* **48**, 225-250. doi:10.1016/S0091-679X(08)61390-4

Barr, M. M., García, L. R. and Portman, D. S. (2018). Sexual dimorphism and sex differences in *Caenorhabditis elegans* neuronal development and behavior. *Genetics* **208**, 909-935. doi:10.1534/genetics.117.300294

Baylis, H. A., Furuichi, T., Yoshikawa, F., Mikoshiba, K. and Sattelle, D. B. (1999). Inositol 1,4,5-trisphosphate receptors are strongly expressed in the nervous system, pharynx, intestine, gonad and excretory cell of *Caenorhabditis elegans* and are encoded by a single gene (*itr*-1). *J. Mol. Biol.* **294**, 467-476. doi:10.1006/jmbi.1999.3229

Brenner, S. (1974). The genetics of *Caenorhabditis elegans*. *Genetics* **77**, 71-94.

Burkewitz, K., Morantte, I., Weir, H. J. M., Yeo, R., Zhang, Y., Huynh, F. K., Ilkayeva, O. R., Hirschey, M. D., Grant, A. R. and Mair, W. B. (2015). Neuronal CRTC-1 governs systemic mitochondrial metabolism and lifespan via a catecholamine signal. *Cell* **160**, 842-855. doi:10.1016/j.cell.2015.02.004

Chen, X. and García, L. R. (2015). Developmental alterations of the *C. elegans* male anal depressor morphology and function require sex-specific cell autonomous and cell non-autonomous interactions. *Dev. Biol.* **398**, 24-43. doi:10.1016/j.ydbio.2014.11.004

Correa, P., LeBoeuf, B. and Garcia, L. R. (2012). *C. elegans* dopaminergic D2-like receptors delimit recurrent cholinergic-mediated motor programs during a goal-oriented behavior. *PLoS Genet.* **8**, e1003015. doi:10.1371/journal.pgen.1003015

Dickinson, D. J., Ward, J. D., Reiner, D. J. and Goldstein, B. (2013). Engineering the *Caenorhabditis elegans* genome using Cas9-triggered homologous recombination. *Nat. Methods* **10**, 1028-1034. doi:10.1038/nmeth.2641

Dolmetsch, R. E., Lewis, R. S., Goodnow, C. C. and Healy, J. I. (1997). Differential activation of transcription factors induced by Ca^{2+} response amplitude and duration. *Nature* **386**, 855-858. doi:10.1038/386855a0

Egan, C. R., Chung, M. A., Allen, F. L., Heschl, M. F. P., Van Buskirk, C. L. and McGhee, J. D. (1995). A gut-to-pharynx/tail switch in embryonic expression of the *Caenorhabditis elegans ges-1* gene centers on two GATA sequences. *Dev. Biol.* **170**, 397-419. doi:10.1006/dbio.1995.1225

Freire, A. G., Resende, T. P. and Pinto-do-Ó, P. (2014). Building and repairing the heart: what can we learn from embryonic development? *BioMed Res. Int.* **2014**, 679168. doi:10.1155/2014/679168

Fu, W.-B., Wang, W. E. and Zeng, C.-Y. (2019). Wnt signaling pathways in myocardial infarction and the therapeutic effects of Wnt pathway inhibitors. *Acta Pharmacol. Sin.* **40**, 9-12. doi:10.1038/s41401-018-0060-4

Garcia, L. R., Mehta, P. and Sternberg, P. W. (2001). Regulation of distinct muscle behaviors controls the *C. elegans* male's copulatory spicules during mating. *Cell* **107**, 777-788. doi:10.1016/S0092-8674(01)00600-6

Gettner, S. N., Kenyon, C. and Reichardt, L. F. (1995). Characterization of beta *pat*-3 heterodimers, a family of essential integrin receptors in *C. elegans*. *J. Cell Biol.* **129**, 1127-1141. doi:10.1083/jcb.129.4.1127

Gower, N. J. D., Walker, D. S. and Baylis, H. A. (2005). Inositol 1,4,5-trisphosphate signaling regulates mating behavior in *Caenorhabditis elegans* males. *Mol. Biol. Cell* **16**, 3978-3986. doi:10.1091/mbc.e05-02-0096

Graef, I. A., Gastier, J. M., Francke, U. and Crabtree, G. R. (2001). Evolutionary relationships among Rel domains indicate functional diversification by recombination. *Proc. Natl. Acad. Sci. USA* **98**, 5740-5745. doi:10.1073/pnas.101602398

Guo, X., Navetta, A., Gualberto, D. G. and García, L. R. (2012). Behavioral decay in aging male *C. elegans* correlates with increased cell excitability. *Neurobiol. Aging* **33**, 1483.e5-1483.e23. doi:10.1016/j.neurobiolaging.2011.12.016

Harfe, B. D., Vaz Gomes, A., Kenyon, C., Liu, J., Krause, M. and Fire, A. (1998). Analysis of a *Caenorhabditis elegans* Twist homolog identifies conserved and divergent aspects of mesodermal patterning. *Genes Dev.* **12**, 2623-2635. doi:10.1101/gad.12.16.2623

Hart, A. C., Sims, S. and Kaplan, J. M. (1995). Synaptic code for sensory modalities revealed by *C. elegans* GLR-1 glutamate receptor. *Nature* **378**, 82-85. doi:10.1038/378082a0

Harterink, M., Kim, D. H., Middelkoop, T. C., Doan, T. D., van Oudenaarden, A. and Korswagen, H. C. (2011). Neuroblast migration along the anteroposterior axis of *C. elegans* is controlled by opposing gradients of Wnts and a secreted Frizzled-related protein. *Development* **138**, 2915-2924. doi:10.1242/dev.064733

Herman, M. A., Vassilieva, L. L., Horvitz, H. R., Shaw, J. E. and Herman, R. K. (1995). The *C. elegans* gene *lin*-44, which controls the polarity of certain asymmetric cell divisions, encodes a Wnt protein and acts cell nonautonomously. *Cell* **83**, 101-110. doi:10.1016/0092-8674(95)90238-4

Hodgkin, J., Horvitz, H. R. and Brenner, S. (1979). Nondisjunction mutants of the nematode *Caenorhabditis elegans*. *Genetics* **91**, 67-94.

Hunt-Newbury, R., Viveiros, R., Johnsen, R., Mah, A., Anastas, D., Fang, L., Halfnight, E., Lee, D., Lin, J., Lorch, A. et al. (2007). High-throughput in vivo analysis of gene expression in *Caenorhabditis elegans*. *PLoS Biol.* **5**, e237-e237. doi:10.1371/journal.pbio.0050237

Jarrell, T. A., Wang, Y., Bloniarz, A. E., Brittin, C. A., Xu, M., Thomson, J. N., Albertson, D. G., Hall, D. H. and Emmons, S. W. (2012). The connectome of a decision-making neural network. *Science* **337**, 437-444. doi:10.1126/science.1221762

Jee, C., Choi, T.-W., Kalichamy, K., Yee, J. Z., Song, H.-O., Ji, Y. J., Lee, J., Lee, J. I., L'Etoile, N. D., Ahnn, J. et al. (2012). CNP-1 (ARRD-17), a novel substrate of calcineurin, is critical for modulation of egg-laying and locomotion in response to food and lysine sensation in *Caenorhabditis elegans*. *J. Mol. Biol.* **417**, 165-178. doi:10.1016/j.jmb.2012.01.012

Kamath, R. S., Martinez-Campos, M., Zipperlen, P., Fraser, A. G. and Ahringer, J. (2001). Effectiveness of specific RNA-mediated interference through ingested double-stranded RNA in *Caenorhabditis elegans*. *Genome Biol.* **2**, Research0002.

Katanaev, V. L., Ponzielli, R., Sémériva, M. and Tomlinson, A. (2005). Trimeric G protein-dependent frizzled signaling in *Drosophila*. *Cell* **120**, 111-122. doi:10.1016/j.cell.2004.11.014

Kirszenblat, L., Pattabiraman, D. and Hilliard, M. A. (2011). LIN-44/Wnt directs dendrite outgrowth through LIN-17/Frizzled in *C. elegans* Neurons. *PLoS Biol.* **9**, e1001157. doi:10.1371/journal.pbio.1001157

Kuhara, A., Inada, H., Katsura, I. and Mori, I. (2002). Negative regulation and gain control of sensory neurons by the *C. elegans* calcineurin TAX-6. *Neuron* **33**, 751-763. doi:10.1016/S0896-6273(02)00607-4

Kuhl, M., Sheldahl, L. C., Malbon, C. C. and Moon, R. T. (2000). Ca(2+)/calmodulin-dependent protein kinase II is stimulated by Wnt and Frizzled homologs and promotes ventral cell fates in Xenopus. *J. Biol. Chem.* **275**, 12701-12711. doi:10.1074/jbc.275.17.12701

Lackner, M. R., Nurrish, S. J. and Kaplan, J. M. (1999). Facilitation of synaptic transmission by EGL-30 Gqα and EGL-8 PLCβ: DAG binding to UNC-13 is required to stimulate acetylcholine release. *Neuron* **24**, 335-346. doi:10.1016/S0896-6273(00)80848-X

LeBoeuf, B. and Garcia, L. R. (2017). *Caenorhabditis elegans* Male Copulation Circuitry Incorporates Sex-Shared Defecation Components To Promote Intromission and Sperm Transfer. *G3* **7**, 647-662. doi:10.1534/g3.116.036756

LeBoeuf, B., Guo, X. and García, L. R. (2011). The effects of transient starvation persist through direct interactions between CaMKII and *ether-a-go-go* K+ channels in *C. elegans* males. *Neuroscience* **175**, 1-17. doi:10.1016/j.neuroscience.2010.12.002

Lee, R. Y. N., Lobel, L., Hengartner, M., Horvitz, H. R. and Avery, L. (1997). Mutations in the alpha1 subunit of an L-type voltage-activated Ca^{2+} channel cause myotonia in *Caenorhabditis elegans*. *EMBO J.* **16**, 6066-6076. doi:10.1093/emboj/16.20.6066

Lee, J., Song, H.-O., Jee, C., Vanoaica, L. and Ahnn, J. (2005). Calcineurin regulates enteric muscle contraction through EXP-1, excitatory GABA-gated channel, in *C. elegans*. *J. Mol. Biol.* **352**, 313-318. doi:10.1016/j.jmb.2005.07.032

Mahoney, T. R., Luo, S., Round, E. K., Brauner, M., Gottschalk, A., Thomas, J. H. and Nonet, M. L. (2008). Intestinal signaling to GABAergic neurons regulates a rhythmic behavior in *Caenorhabditis elegans*. *Proc. Natl Acad. Sci. USA* **105**, 16350-16355. doi:10.1073/pnas.0803617105

Mair, W., Morantte, I., Rodrigues, A. P. C., Manning, G., Montminy, M., Shaw, R. J. and Dillin, A. (2011). Lifespan extension induced by AMPK and calcineurin is mediated by CRTC-1 and CREB. *Nature* **470**, 404-408. doi:10.1038/nature09706

Maricq, A. V., Peckol, E., Driscoll, M. and Bargmann, C. I. (1995). Mechanosensory signalling in *C. elegans* mediated by the GLR-1 glutamate receptor. *Nature* **378**, 78-81. doi:10.1038/378078a0

Maryon, E. B., Coronado, R. and Anderson, P. (1996). *unc*-68 encodes a ryanodine receptor involved in regulating *C. elegans* body-wall muscle contraction. *J. Cell Biol.* **134**, 885-893. doi:10.1083/jcb.134.4.885

McQuate, A., Latorre-Esteves, E. and Barria, A. (2017). A Wnt/Calcium signaling cascade regulates neuronal excitability and trafficking of NMDARs. *Cell Rep.* **21**, 60-69. doi:10.1016/j.celrep.2017.09.023

Mello, C. and Fire, A. (1995). DNA transformation. *Methods Cell Biol.* **48**, 451-482. doi:10.1016/S0091-679X(08)61399-0

Mendel, J. E., Korswagen, H. C., Liu, K. S., Hajdu-Cronin, Y. M., Simon, M. I., Plasterk, R. H. and Sternberg, P. W. (1995). Participation of the protein Go in multiple aspects of behavior in *C. elegans*. *Science* **267**, 1652-1655. doi:10.1126/science.7886455

Meng, L., Mulcahy, B., Cook, S. J., Neubauer, M., Wan, A., Jin, Y. and Yan, D. (2015). The cell death pathway regulates synapse elimination through cleavage of Gelsolin in *Caenorhabditis elegans* neurons. *Cell Rep.* **11**, 1737-1748. doi:10.1016/j.celrep.2015.05.031

Miller, K. G., Emerson, M. D. and Rand, J. B. (1999). Goα and diacylglycerol kinase negatively regulate the Gqα pathway in *C. elegans*. *Neuron* **24**, 323-333. doi:10.1016/S0896-6273(00)80847-8

Miller-Fleming, T. W., Petersen, S. C., Manning, L., Matthewman, C., Gornet, M., Beers, A., Hori, S., Mitani, S., Bianchi, L., Richmond, J. et al. (2016). The DEG/ENaC cation channel protein UNC-8 drives activity-dependent synapse removal in remodeling GABAergic neurons. *eLife* **5**, e14599. doi:10.7554/eLife.14599

Nakai, J., Ohkura, M. and Imoto, K. (2001). A high signal-to-noise Ca(2+) probe composed of a single green fluorescent protein. *Nat. Biotechnol.* **19**, 137-141. doi:10.1038/84397

Pan, C.-L., Howell, J. E., Clark, S. G., Hilliard, M., Cordes, S., Bargmann, C. I. and Garriga, G. (2006). Multiple Wnts and frizzled receptors regulate anteriorly directed cell and growth cone migrations in *Caenorhabditis elegans*. *Dev. Cell* **10**, 367-377. doi:10.1016/j.devcel.2006.02.010

Pani, A. M. and Goldstein, B. (2018). Direct visualization of a native Wnt in vivo reveals that a long-range Wnt gradient forms by extracellular dispersal. *eLife* **7**, e38325. doi:10.7554/eLife.38325

Park, D., Jhon, D. Y., Lee, C. W., Lee, K. H. and Rhee, S. G. (1993). Activation of phospholipase C isozymes by G protein beta gamma subunits. *J. Biol. Chem.* **268**, 4573-4576.

Parra, V. and Rothermel, B. A. (2017). Calcineurin signaling in the heart: the importance of time and place. *J. Mol. Cell. Cardiol.* **103**, 121-136. doi:10.1016/j.yjmcc.2016.12.006

Paudel, S., Sindelar, R. and Saha, M. (2018). Calcium signaling in vertebrate development and its role in disease. *Int. J. Mol. Sci.* **19**, 3390. doi:10.3390/ijms19113390

Pénigault, J. B. and Félix, M. A. (2011). High sensitivity of *C. elegans* vulval precursor cells to the dose of posterior Wnts. *Dev. Biol.* **357**, 428-438. doi:10.1016/j.ydbio.2011.06.006

Prömel, S., Fiedler, F., Binder, C., Winkler, J., Schöneberg, T. and Thor, D. (2016). Deciphering and modulating G protein signalling in *C. elegans* using the DREADD technology. *Sci. Rep.* **6**, 28901. doi:10.1038/srep28901

Reiner, D. J. and Thomas, J. H. (1995). Reversal of a muscle response to GABA during *C. elegans* male development. *J. Neurosci.* **15**, 6094-6102. doi:10.1523/JNEUROSCI.15-09-06094.1995

Reiner, D. J., Weinshenker, D., Tian, H., Thomas, J. H., Nishiwaki, K., Miwa, J., Gruninger, T., Leboeuf, B. and Garcia, L. R. (2006). Behavioral genetics of *Caenorhabditis elegans unc*-103-encoded erg-like K(+) channel. *J. Neurogenet.* **20**, 41-66. doi:10.1080/01677060600788826

Saneyoshi, T., Kume, S., Amasaki, Y. and Mikoshiba, K. (2002). The Wnt/calcium pathway activates NF-AT and promotes ventral cell fate in Xenopus embryos. *Nature* **417**, 295-299. doi:10.1038/417295a

Sawa, H. and Korswagen, H. C. (2013). Wnt signaling in *C. elegans*. *WormBook* 1-30. doi: 10.1895/wormbook.1.7.2.

Sawa, H., Lobel, L. and Horvitz, H. R. (1996). The *Caenorhabditis elegans* gene *lin*-17, which is required for certain asymmetric cell divisions, encodes a putative seven-transmembrane protein similar to the Drosophila frizzled protein. *Genes Dev.* **10**, 2189-2197. doi:10.1101/gad.10.17.2189

Schnabel, H. and Schnabel, R. (1990). An organ-specific differentiation gene, *pha-1*, from *Caenorhabditis elegans*. *Science* **250**, 686-688. doi:10.1126/science.250.4981.686

Sheldahl, L. C., Park, M., Malbon, C. C. and Moon, R. T. (1999). Protein kinase C is differentially stimulated by Wnt and Frizzled homologs in a G-protein-dependent manner. *Curr. Biol.* **9**, 695-698. doi:10.1016/S0960-9822(99)80310-8

Shimizu, H., Langenbacher, A. D., Huang, J., Wang, K., Otto, G., Geisler, R., Wang, Y. and Chen, J.-N. (2017). The Calcineurin-FoxO-MuRF1 signaling pathway regulates myofibril integrity in cardiomyocytes. *eLife* **6**, e27955. doi:10.7554/eLife.27955

Slusarski, D. C., Corces, V. G. and Moon, R. T. (1997). Interaction of Wnt and a Frizzled homologue triggers G-protein-linked phosphatidylinositol signalling. *Nature* **390**, 410-413. doi:10.1038/37138

Sulston, J. E. and Horvitz, H. R. (1977). Post-embryonic cell lineages of the nematode, *Caenorhabditis elegans*. *Dev. Biol.* **56**, 110-156. doi:10.1016/0012-1606(77)90158-0

Sulston, J. E., Albertson, D. G. and Thomson, J. N. (1980). The *Caenorhabditis elegans* male: postembryonic development of nongonadal structures. *Dev. Biol.* **78**, 542-576. doi:10.1016/0012-1606(80)90352-8

Takeshita, H. and Sawa, H. (2005). Asymmetric cortical and nuclear localizations of WRM-1/beta-catenin during asymmetric cell division in C. elegans. *Genes Dev.* **19**, 1743-1748. doi:10.1101/gad.1322805

Tao, L., Xie, Q., Ding, Y.-H., Li, S.-T., Peng, S., Zhang, Y.-P., Tan, D., Yuan, Z. and Dong, M.-Q. (2013). CAMKII and calcineurin regulate the lifespan of *Caenorhabditis elegans* through the FOXO transcription factor DAF-16. *eLife* **2**, e00518. doi:10.7554/eLife.00518.029

Thomas, J. H. (1990). Genetic analysis of defecation in *Caenorhabditis elegans*. *Genetics* **124**, 855-872.

Tian, L., Hires, S. A., Mao, T., Huber, D., Chiappe, M. E., Chalasani, S. H., Petreanu, L., Akerboom, J., McKinney, S. A., Schreiter, E. R. et al. (2009). Imaging neural activity in worms, flies and mice with improved GCaMP calcium indicators. *Nat. Methods* **6**, 875-881. doi:10.1038/nmeth.1398

Walker, D. S., Vázquez-Manrique, R. P., Gower, N. J. D., Gregory, E., Schafer, W. R. and Baylis, H. A. (2009). Inositol 1,4,5-trisphosphate signalling regulates the avoidance response to nose touch in *Caenorhabditis elegans*. *PLoS Genet.* **5**, e1000636. doi:10.1371/journal.pgen.1000636

Whangbo, J. and Kenyon, C. (1999). A Wnt signaling system that specifies two patterns of cell migration in *C. elegans*. *Mol. Cell* **4**, 851-858. doi:10.1016/S1097-2765(00)80394-9

Wicks, S. R., Yeh, R. T., Gish, W. R., Waterston, R. H. A. and Plasterk, R. H. (2001). Rapid gene mapping in *Caenorhabditis elegans* using a high density polymorphism map. *Nat. Genet.* **28**, 160-164. doi:10.1038/88878

Wu, M. and Herman, M. A. (2006). A novel noncanonical Wnt pathway is involved in the regulation of the asymmetric B cell division in *C. elegans*. *Dev. Biol.* **293**, 316-329. doi:10.1016/j.ydbio.2005.12.024

Wu, M. and Herman, M. A. (2007). Asymmetric localizations of LIN-17/Fz and MIG-5/Dsh are involved in the asymmetric B cell division in *C. elegans*. *Dev. Biol.* **303**, 650-662. doi:10.1016/j.ydbio.2006.12.002

Xu, S. and Chisholm, A. D. (2011). A Gαq-Ca^{2+} signaling pathway promotes actin-mediated epidermal wound closure in *C. elegans*. *Curr. Biol.* **21**, 1960-1967. doi:10.1016/j.cub.2011.10.050

Yoshida, Y., Kim, S., Chiba, K., Kawai, S., Tachikawa, H. and Takahashi, N. (2004). Calcineurin inhibitors block dorsal-side signaling that affect late-stage development of the heart, kidney, liver, gut and somitic tissue during Xenopus embryogenesis. *Dev. Growth Differ.* **46**, 139-152. doi:10.1111/j.1440-169X.2004.00733.x

Zhao, G., Qiu, Y., Zhang, H. M. and Yang, D. (2019). Intercalated discs: cellular adhesion and signaling in heart health and diseases. *Heart Fail. Rev.* **24**, 115-132. doi:10.1007/s10741-018-9743-7

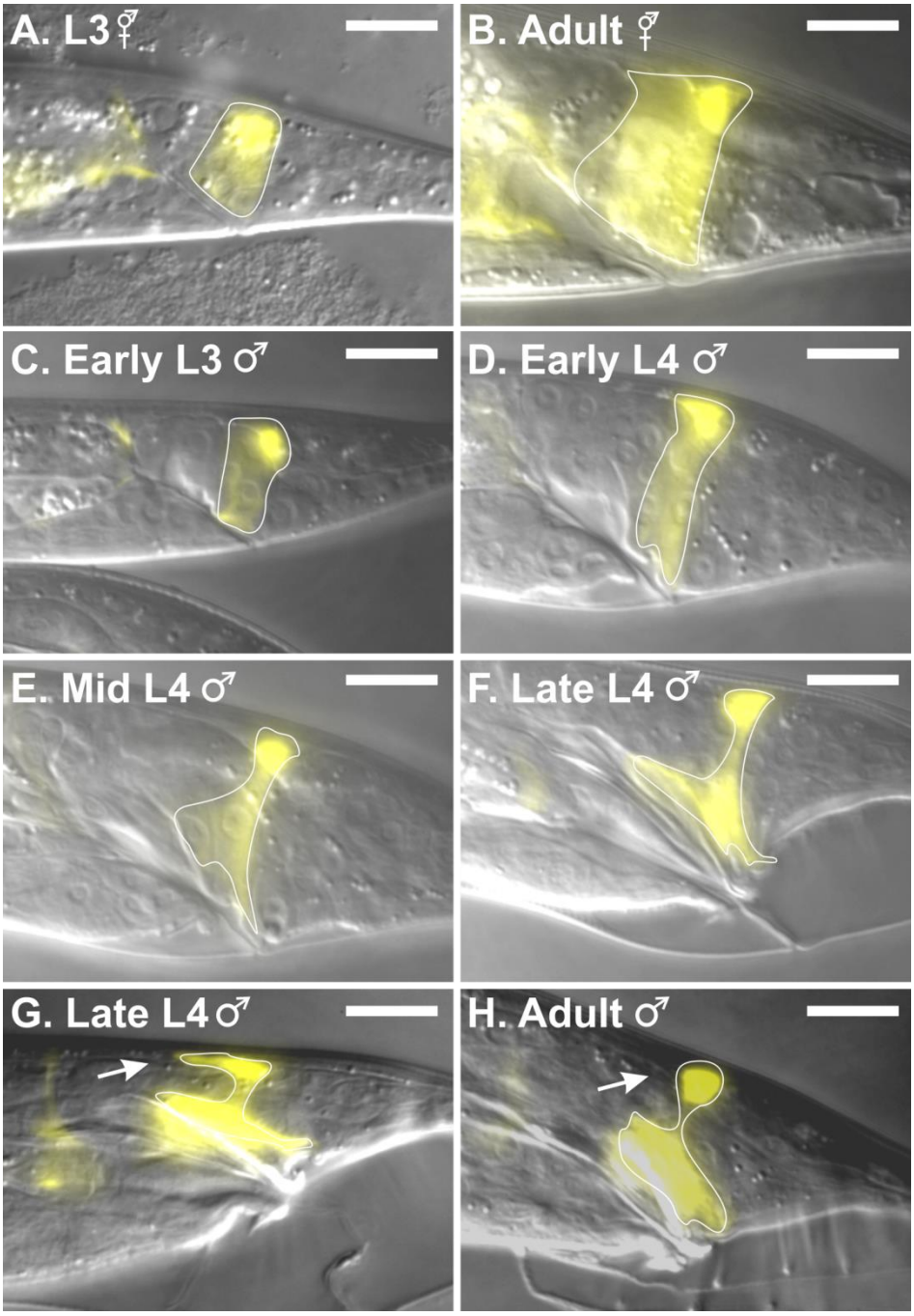

Figure S1. Visualization of male anal depressor remodeling during development using cytoplasmic YFP. The anal depressor is outline in white. Each image is a DIC image overlaid with a fluorescent image of the anal depressor. (A-B) Hermaphrodite. (C-H) Male. The arrows in G and H indicate the location of the nucleus. Scale bar = 10 µm.

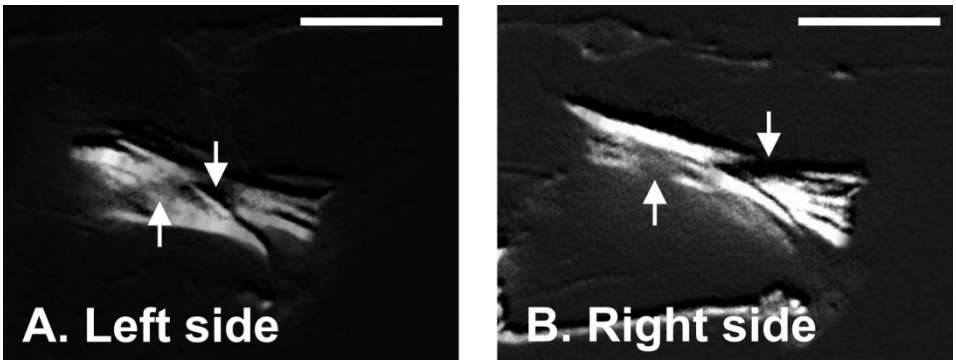

Figure S2. Double sarcomere on left and right side of adult male anal depressor. The arrows point to the two distinct gaps (putative H zone) that separate the anterior-posterior actin filaments. Scale bar = 10 µm.

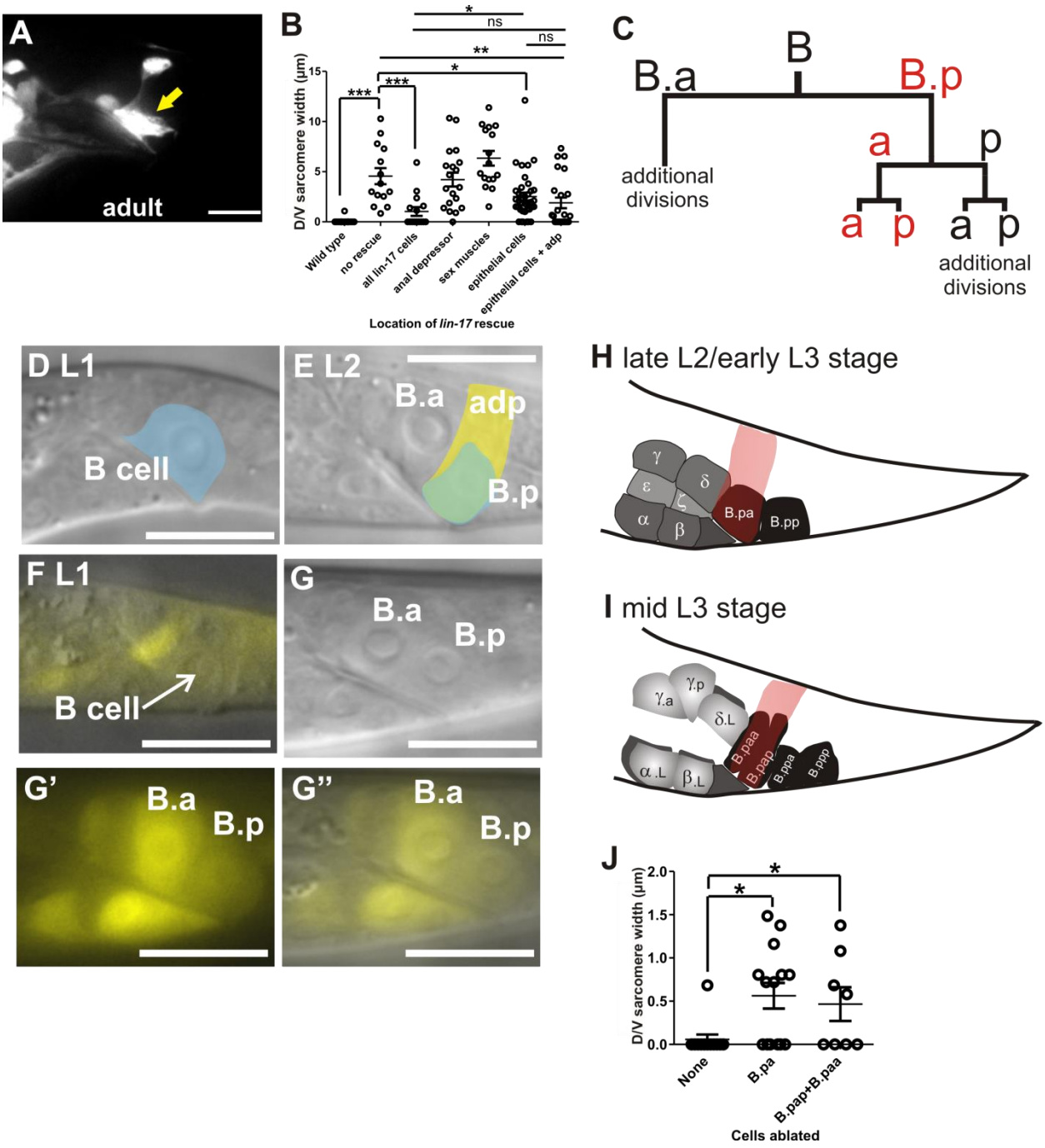

Figure S3. Role of frizzled/LIN-17 receptor in development of the male tail

(A) P*lin-17*:YFP expression pattern in an adult male. Yellow arrow indicates the anal depressor. Scale bar = 10 µm.

(B) Graph depicting dorsal/ventral sarcomere width in *lin-17* mutants that have been rescued with *lin-17* cDNA in the indicated locations. Each dot represents the dorsal/ventral sarcomere width of either the left or right dorsal attachment in one male. Mean ±SE is indicated. n.s. = not significant, *p<0.05, **p<0.005, ***p<0.0001, Mann Whitney t test.

(C) Diagram of B cell divisions. a=anterior, p=posterior. Red fonts refer to B-derived cells that contact the anal depressor.

(D) DIC image of L1 male. B cell highlighted in light blue.

(E) DIC image of a L2 male. B.p cell highlighted in light green. Location of anal depressor shown in yellow.

(F) A DIC image of an L1 male tail overlaid with a P*pop-1*:YFP fluorescent image. The location of the B cell is indicated by the white arrow. The anal depressor does not express P*pop-1*:YFP.

(G) DIC image of L2 male tail. G' is P*pop-1*:YFP fluorescent image in the L2 male tail. G'' is the overlay of the (G) DIC and (G') fluorescent images, showing the expression of P*pop-1*:YFP in the B cell descendants.

(H,I) Cartoon of a late L2/early L3 and mid L3 male tail depicting the positions of the anal depressor (pink) and B.a cell descendants (shades of grey) and B.p cell descendants (black).

(J) Graph depicting dorsal/ventral sarcomere width in males that have had B cell descendants ablated. Each dot represents the dorsal/ventral sarcomere width of either the left or right dorsal attachment in one male. Mean ±SE is indicated. *p<0.05, Mann Whitney t test.

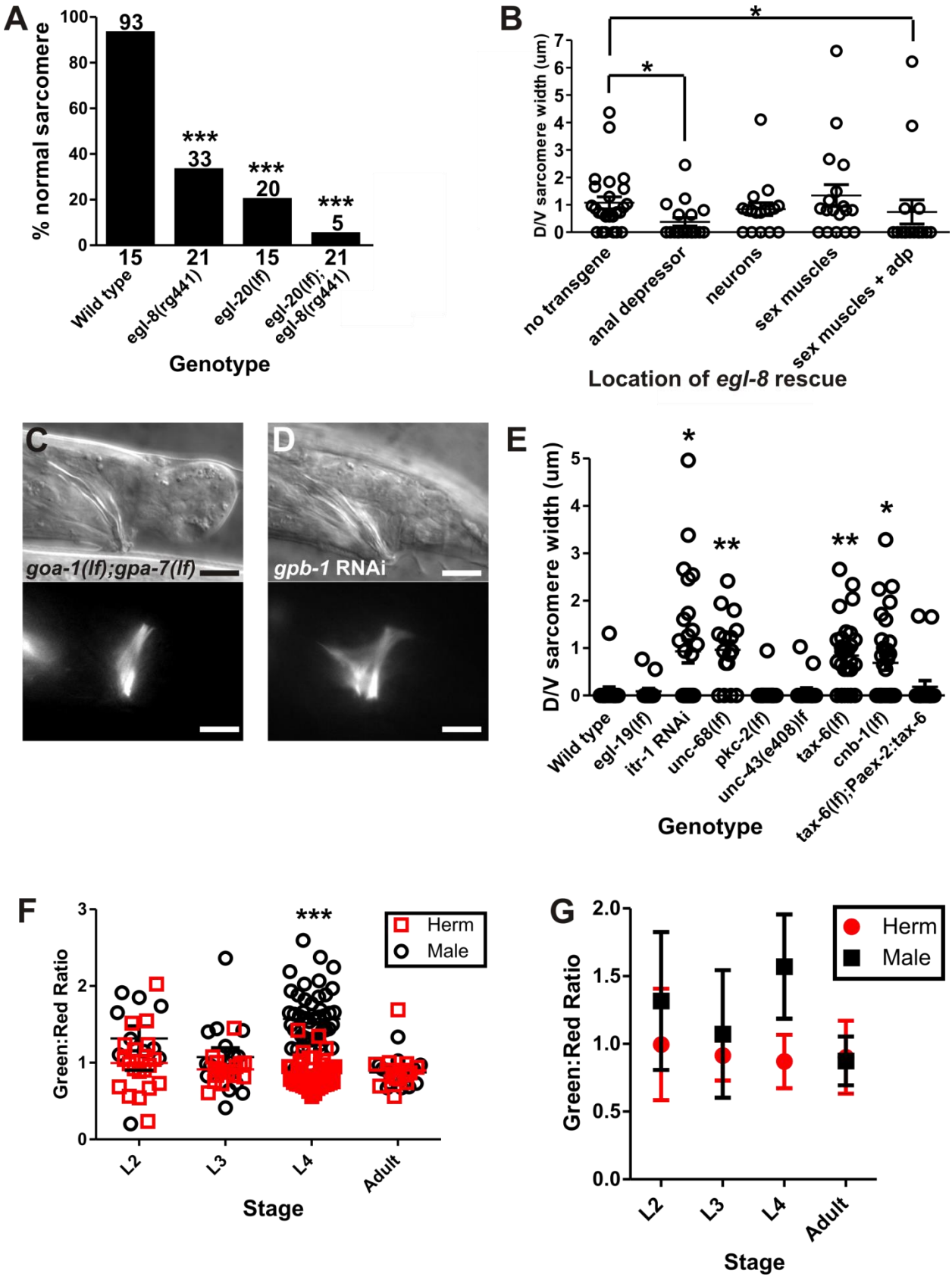

Figure S4. Role of calcium in anal depressor rearrangement

(A) Graph depicting the percentage of males (number above the bar) that have normal sarcomeres in the indicated mutants. Number below the x-axis is the *n*. ***p<0.0001, Fisher's exact test, compared to wild type.

(B) Graph depicting dorsal-ventral sarcomere width in *egl-8* mutant males that have been rescued with an *egl-8* minigene in the indicated locations. x-axis indicates where the *egl-8* minigene is expressed. Each dot represents the dorsal-ventral sarcomere width of either the left or right dorsal attachment in one male. Mean ±SE is indicated. *p<0.05, Mann Whitney t test.

(C,D) DIC (top) and YFP:actin (bottom) fluorescent image of adult male tail and anal depressor, respectively. Dorsal is top, anterior is to the left. Scale bar = 10 µm.

(E) Graph depicting dorsal-ventral sarcomere width in males that have mutations in calcium pathway genes. Each dot represents the dorsal-ventral sarcomere width of either the left or right dorsal attachment in one male. Mean ±SE is indicated. *p<0.05, **p<0.005, Mann Whitney t test, compared to wild type. *itr-1* RNAi and *pkc-2(lf)* were scored using an P*unc-103*E:YFP:actin expressing transgene (Chen and García, 2015).

(F) Graph depicting fluorescent levels over different developmental stages (x axis). Each individual dot represents one worm. ***p<0.0001, Mann Whitney t test.

(G) The data in (F) represented as average (dot) and standard deviation (lines).

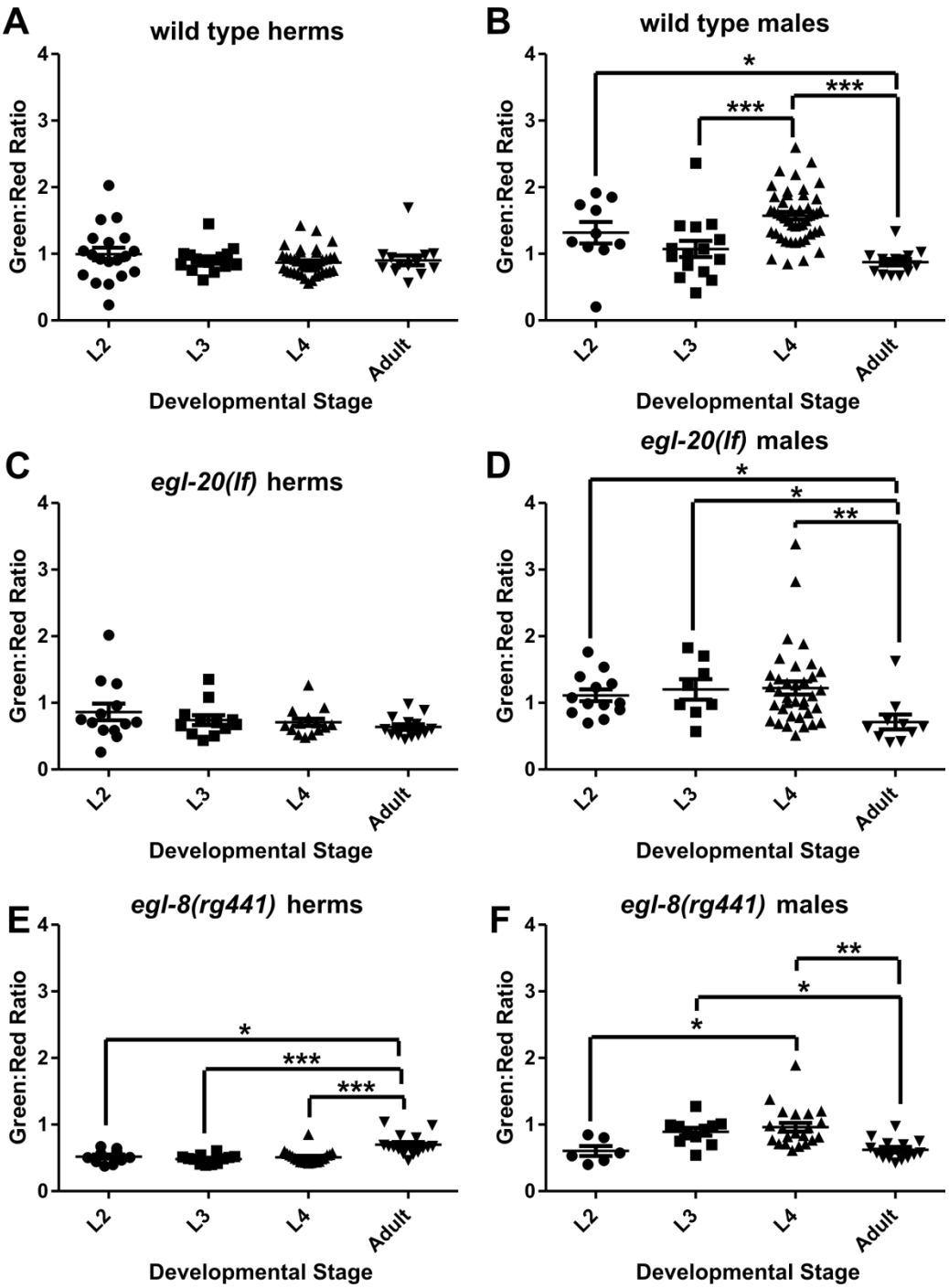

Figure S5. Anal depressor calcium levels through different developmental stages.

(A-F) Graphs depicting fluorescent levels over different developmental stages (x axis). Each individual dot represents one worm. *p<0.05, **p<0.005, ***p<0.0001, Mann Whitney t test.

Table S1. Resources

Click here to Download Table S1